RESEARCH ARTICLE

Emergence of belief-like representations through reinforcement learning

Jay A. Hennig[1,2]*, **Sandra A. Romero Pinto**[2,3,4], **Takahiro Yamaguchi**[3,5], **Scott W. Linderman**[6,7], **Naoshige Uchida**[2,3], **Samuel J. Gershman**[1,2]

1 Department of Psychology, Harvard University, Cambridge, Massachusetts, United States of America, **2** Center for Brain Science, Harvard University, Cambridge, Massachusetts, United States of America, **3** Department of Molecular and Cellular Biology, Harvard University, Cambridge, Massachusetts, United States of America, **4** Program in Speech and Hearing Bioscience and Technology, Harvard Medical School, Boston, Massachusetts, USA, **5** Future Research Department, Toyota Research Institute of North America, Toyota Motor North America, Ann Arbor, Michigan, United States of America, **6** Wu Tsai Neurosciences Institute, Stanford University, Stanford, California, United States of America, **7** Department of Statistics, Stanford University, Stanford, California, United States of America

* jay.a.hennig@gmail.com

Abstract

To behave adaptively, animals must learn to predict future reward, or value. To do this, animals are thought to learn reward predictions using reinforcement learning. However, in contrast to classical models, animals must learn to estimate value using only incomplete state information. Previous work suggests that animals estimate value in partially observable tasks by first forming "beliefs"—optimal Bayesian estimates of the hidden states in the task. Although this is one way to solve the problem of partial observability, it is not the only way, nor is it the most computationally scalable solution in complex, real-world environments. Here we show that a recurrent neural network (RNN) can learn to estimate value directly from observations, generating reward prediction errors that resemble those observed experimentally, without any explicit objective of estimating beliefs. We integrate statistical, functional, and dynamical systems perspectives on beliefs to show that the RNN's learned representation encodes belief information, but only when the RNN's capacity is sufficiently large. These results illustrate how animals can estimate value in tasks without explicitly estimating beliefs, yielding a representation useful for systems with limited capacity.

Author summary

Natural environments are full of uncertainty. For example, just because my fridge had food in it yesterday does not mean it will have food today. Despite such uncertainty, animals can estimate which states and actions are the most valuable. Previous work suggests that animals estimate value using a brain area called the basal ganglia, using a process resembling a reinforcement learning algorithm called TD learning. However, traditional reinforcement learning algorithms cannot accurately estimate value in environments with state uncertainty (e.g., when my fridge's contents are unknown). One way around this problem is if agents form "beliefs," a probabilistic estimate of how likely each state is,

given any observations so far. However, estimating beliefs is a demanding process that may not be possible for animals in more complex environments. Here we show that an artificial recurrent neural network (RNN) trained with TD learning can estimate value from observations, without explicitly estimating beliefs. The trained RNN's error signals resembled the neural activity of dopamine neurons measured during the same tasks. Importantly, the RNN's activity resembled beliefs, but only when the RNN had enough capacity. This work illustrates how animals could estimate value in uncertain environments without needing to first form beliefs, which may be useful in environments where computing the true beliefs is too costly.

Introduction

One pervasive feature of animal behavior is the ability to predict future reward. For example, a dog may learn that when her owner picks up the leash, she is likely to be rewarded with a walk in the near future. In associative learning settings such as this one, animals learn to associate certain stimuli (e.g., the owner grabbing the leash) with future reward (e.g., a walk). The neural basis of associative learning has been interpreted through the lens of reinforcement learning (RL). In particular, one successful theoretical model posits that associative learning is driven by the activity of dopamine neurons in the midbrain, where spiking activity resembles the reward prediction error (RPE) signal in an RL algorithm called temporal difference (TD) learning [1–4]. We will describe this algorithm in more detail below.

In many real-world scenarios, effectively predicting reward may require a deeper understanding of the structure of the world that goes beyond associating observations and reward. To continue the example above, suppose the dog's owner keeps his car keys under the leash. Now if he picks up the leash, this does not necessarily mean he is about to take his dog on a walk. As a result, his intention to take his dog on a walk is now "partially observable." Standard RL approaches are insufficient for learning in partially observable environments, as these methods assume that all relevant states of the environment are fully observable. One way to solve this problem is by using observations to form a Bayesian posterior estimate of each hidden state, called a *belief state* [5]. Future reward can then be estimated by applying standard RL methods like TD learning to belief states rather than the raw observations.

Do animals estimate future reward using belief states? Evidence for this idea is suggestive, although indirect. Previous experimental work has shown that the phasic activity of midbrain dopamine neurons resembles the RPEs of TD learning in partially observable environments, where TD learning is performed on belief states rather than observations [6–11]. The brain may have dedicated machinery, perhaps in prefrontal cortex [12, 13], for computing belief states, which could then be provided to downstream areas, such as the basal ganglia, to perform standard RL algorithms such as TD learning [14]. This architectural division of labor resonates with the broader literature on probabilistic computation in cortex, which has identified several different ways in which belief states could be encoded by neural activity [15].

There are a few difficulties in using a belief state to solve RL tasks. First, the belief state assumes knowledge of the environment's transition and observation dynamics—something that may be challenging for animals to acquire via observations alone. Indeed, there are well-documented examples of animals failing to learn or use the correct environment model [16]. Second, the belief representation does not scale well to more realistic tasks with higher-dimensional state spaces, as beliefs live in a continuous space whose dimensionality grows with the number of discrete states in the environment. Finally, the belief state includes knowledge

about all states in the environment, regardless of whether or not those states are relevant to the task at hand. Luckily, one can often use approximate representations of beliefs to find solutions that work well in practice [17]. This suggests that there may be other representations that are sufficient for the particular task of estimating future reward, but easier to compute than the full belief state [18, 19].

To address these difficulties, here we take inspiration from deep reinforcement learning. In deep RL, rather than explicitly learning beliefs, an agent uses nonlinear function approximation to learn a hidden representation that is sufficient for performing the task [20]. Compared to the belief representation, this approach does not require explicit knowledge about the structure of the environment. It may also scale better to more complex tasks, by virtue of the agent not needing to represent any features of the environment that do not directly pertain to the task at hand. Because beliefs are a non-linear dynamical system, here we use recurrent neural networks (RNNs) as our nonlinear function approximator. This choice was also motivated by the observation from the machine learning literature that RNNs can perform well on complex partially observable tasks [21]. Previous work in computational neuroscience has explored whether RNNs can be used to directly compute beliefs [17]. Here, by contrast, we explore whether training RNNs in partially observable environments leads to their representations becoming implicitly more like beliefs.

We first show that RNNs can be trained to optimally estimate value in two previously studied associative learning tasks [7, 10], and that the RPEs of these models resemble experimentally observed dopamine neuron activity. We then probe the representations learned by the RNNs, and find that the learned representations resemble beliefs from statistical, functional, and dynamical systems perspectives. Next, to explore how this approach performs when the RNN's capacity is limited, we characterize how the RNN's representations vary as a function of the RNN's size (i.e., the number of hidden units). We show that the RNN's capacity influences the extent to which its learned representation resembles beliefs, without a concurrent impact on its ability to estimate the value function. Finally, to investigate the importance of letting the RNN's representations be learned during training, we also analyze randomly initialized, untrained RNNs. We find that some untrained RNNs can accurately estimate the value function, and even have representations that partially resemble beliefs. However, only the representations of trained RNNs have representations that resemble beliefs from a dynamical systems perspective. Overall, our work illustrates how animals can estimate reward in partially observable environments without requiring an explicit representation of beliefs, and also identifies multiple signatures of belief-like representations.

Results

Reinforcement learning in partially observable environments using belief states

One standard objective of RL is to learn the expected discounted future return, or *value*, of each state:

$$V(s_t) = \mathbb{E}\left[\sum_{k=0}^{\infty} \gamma^k r_{t+k}\right] \tag{1}$$

where $s_t \in \mathcal{S}$ is the state of the environment at time t, $0 \leq \gamma < 1$ is a discount factor, and r_t is the reward. Rewards are random variables that depend on the environment state, and $\mathbb{E}$ denotes an expectation over the potentially stochastic sequences of states and rewards. For notational simplicity, we will use the shorthand $V_t = V(s_t)$.

Agents do not typically have access to the true value function. Instead, they have an estimate, $\widehat{V}_t$, which they can update over time using sample paths of states and rewards. In TD learning, agents estimate the discrepancy in their estimated value function using a so-called temporal difference error, the precise definition of the RPE used in TD learning:

$$\delta_t = r_t + \gamma \widehat{V}_{t+1} - \widehat{V}_t. \tag{2}$$

where $\mathbb{E}[\delta_t] = 0$ when $\widehat{V}_t = V_t$. In general, we will suppose $\widehat{V}_t$ is determined by a set of adaptable parameters $\boldsymbol{\theta}$. We can improve $\boldsymbol{\theta}$ by following the stochastic gradient of the squared TD error:

$$\Delta\boldsymbol{\theta} = \eta\delta_t\nabla_{\boldsymbol{\theta}}\widehat{V}_t, \tag{3}$$

where $0 < \eta < 1$ is a learning rate, and $\nabla_{\boldsymbol{\theta}}\widehat{V}_t$ is the gradient of $\widehat{V}_t$ with respect to $\boldsymbol{\theta}$.

As for how we construct $\widehat{V}_t$, note that in a partially observable Markov process, agents do not observe the state s_t directly, but instead observe only observations $o_t \in \mathcal{O}$. However, observations are not in general Markovian, which means that $\widehat{V}_t$ cannot be naively written as a function of o_t, but must instead be a function of the entire *history* of observations: $(o_1, \ldots, o_t)$. One way of understanding this is to note that the value of an observation may depend on the long-term past [22]. In the dog leash example from the Introduction, the value (to the dog) of her owner picking up the leash depends on the history of events leading up to that moment—for example, if her owner recently announced that his car keys were missing. To use methods such as TD learning, which assume a Markovian state space, we require a compression of this history into a "sufficient statistic"—that is, a transformed state space over which the Markov property holds. Here we will suppose that, given such a sufficient statistic, $\boldsymbol{z}_t \in \mathbb{R}^D$, we can write $\widehat{V}_t$ as a linear function:

$$\widehat{V}_t = \sum_{d=1}^{D} w(d)z_t(d) = \boldsymbol{w}^{\top}\boldsymbol{z}_t, \tag{4}$$

where $z_t(d) \in \mathbb{R}$ is some feature (indexed by d) summarizing the history of observations, and $\boldsymbol{w} = \boldsymbol{\theta} \in \mathbb{R}^D$ is a learned set of weights on those features. We can learn $\boldsymbol{w}$ using Eq (3) by noting that $\nabla_{\boldsymbol{\theta}}\widehat{V}_t = \boldsymbol{z}_t$, and thus $\Delta\boldsymbol{w} = \eta\delta_t\boldsymbol{z}_t$.

The question is, what is an appropriate sufficient statistic? One standard answer is the posterior probability distribution over hidden states given the history of observations and actions, also known as the *belief state* [5]:

$$b_t(i) = P(s_t = i \mid o_1, \ldots, o_t, a_1, \ldots, a_{t-1})$$

$$\propto P(o_t \mid s_t = i) \sum_{j=1}^{K} P(s_t = i \mid s_{t-1} = j, a_{t-1})\, b_{t-1}(j) \tag{5}$$

which stipulates how to update the belief in state i given observation o_t, and action a_{t-1}. Here we suppose there are K discrete states, though the above equation can be extended naturally to continuous state spaces.

In this study we will consider Pavlovian associative learning tasks, where the sequence of observations and rewards is effectively independent of the agent's actions. As a result, both the beliefs and value function are independent of the agent's actions, and the value function is simply a linear transformation of the beliefs (see Materials and methods). This motivates a straightforward model for estimating value in such partially observable environments [6, 7]: First compute beliefs, and then compute the value estimate as a linear transformation of those

beliefs, with weights updated by TD learning. This model, which we will refer to as the "Belief model", can be written as:

$$\boldsymbol{b}_t \quad = \quad P(s_t \mid \boldsymbol{b}_{t-1}, o_t) \qquad \text{(from Eqn.(5))}$$
$$\widehat{V}_t \quad = \quad \boldsymbol{w}^\top \boldsymbol{b}_t \qquad \text{(substituting } \boldsymbol{b}_t \text{ for } \boldsymbol{z}_t \text{ into Eqn.(4))}$$
$$\Delta \boldsymbol{w} \quad = \quad \eta \delta_t \boldsymbol{b}_t \qquad \text{(from Eqn.(3))}$$

where $\boldsymbol{b}_t \in [0, 1]^K$ is the model's belief over the K discrete states, and only $\boldsymbol{w}$ is learned.

Learning state representations using recurrent neural networks

The Belief model presupposes that animals use a particular feature representation (i.e., beliefs) for estimating value. However, as we described in the Introduction, there are difficulties with assuming animals use a belief representation. Here we ask whether an alternative representation could be learned from the task of estimating value itself, rather than chosen *a priori*. Note that beliefs can be written as follows:

$$\boldsymbol{b}_t = P(s_t \mid o_1, \ldots, o_t) \tag{6}$$
$$= f_\phi(\boldsymbol{b}_{t-1}, o_t)$$

where f is a function parameterized by a specific choice of (fixed) parameters ϕ to ensure the equality holds. This latter equation has the same form as a generic recurrent neural network (RNN). This suggests a model could learn its own representation by treating ϕ as a learnable parameter. We refer to this alternative model as a "Value RNN":

$$\boldsymbol{z}_t = f_\phi(\boldsymbol{z}_{t-1}, o_t) \tag{7}$$

$$\widehat{V}_t = \boldsymbol{w}^\top \boldsymbol{z}_t \tag{8}$$

$$\Delta \boldsymbol{\theta} = \eta \delta_t \nabla_{\boldsymbol{\theta}} \widehat{V}_t \tag{9}$$

where $\boldsymbol{z}_t \in \mathbb{R}^H$ is the activity of an RNN with H hidden units and parameters ϕ, $\boldsymbol{\theta} = [\phi, \boldsymbol{w}]$ is our vector of learned parameters, and $\nabla_{\boldsymbol{\theta}} \widehat{V}_t$ can be calculated using backpropagation through time. The only difference from the Belief model is that the representation, $\boldsymbol{z}_t$, is learned (via ϕ). This allows the network to discover a representation—potentially distinct from beliefs—that is sufficient for estimating value.

Importantly, this RNN-based approach resolves all three challenges for learning a belief representation that we raised in the Introduction: 1) The model can learn from observations alone, as no information is provided about the statistics of the underlying environment; 2) the model's size (parameterized by H, the number of hidden units) can be controlled separately from the number of states in the environment; and 3) the model's only objective is to estimate value. Though such a model has no explicit objective of learning beliefs (its only objective is to estimate value), the network may discover a belief representation implicitly. We next asked what signatures, if any, would indicate the existence of a belief representation. In the sections that follow we develop an analytical approach for determining whether the Value RNN's learned representations resemble beliefs.

RNNs learn belief-like representations

As a working example, we will consider the probabilistic associative learning paradigm where dopamine RPEs were shown to be consistent with a belief representation [7, 13]. This has the
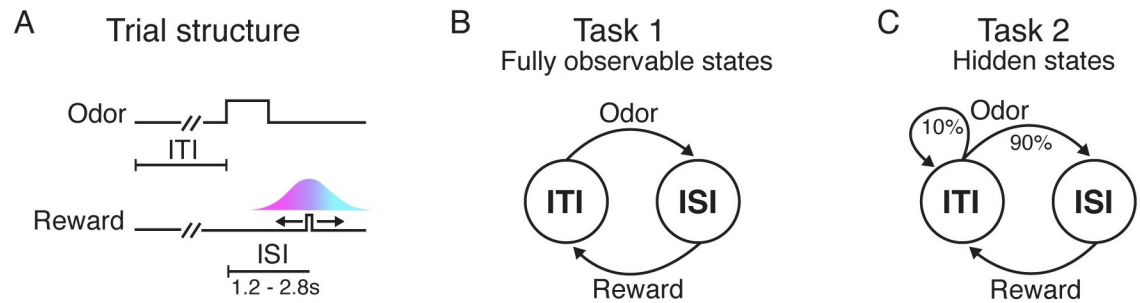
Fig 1. Associative learning tasks with probabilistic rewards and hidden states. A. Trial structure in Starkweather et al. (2017) [7]. Each trial consisted of a variable delay (the intertrial interval, or ITI), followed by an odor, a second delay (the interstimulus interval, or ISI), and a potential subsequent reward. Reward times were sampled from a discretized Gaussian ranging from 1.2–2.8s (see Materials and methods). **B-C.** In both versions of the task, there were two underlying states: the ITI and the ISI. In Task 1, every trial was rewarded. As a result, an odor always indicated a transition from the ITI to the ISI, while a reward always indicated a transition from the ISI to the ITI. In Task 2, rewards were omitted on 10% of trials; as a result, an odor did not reveal whether or not the state transitioned to the ISI.

https://doi.org/10.1371/journal.pcbi.1011067.g001

added benefit of ensuring that the RNN-based approach described above can recapitulate these previous results.

This paradigm consisted of two tasks, which we will refer to as Task 1 and Task 2 (Fig 1). In both tasks, mice were trained to associate an odor cue with probabilistic delivery of a liquid reward 1.2–2.8s later. The tasks were each composed of two states: an intertrial interval (ITI), during which animals waited for an odor; and an interstimulus interval (ISI), during which animals waited for a reward. In Task 1, every trial contained both an odor and a reward. As a result, the animal's observations could fully disambiguate the underlying state: An odor signaled a transition to the ISI state, while a reward signaled a transition to the ITI state. In Task 2, by contrast, reward on a given trial was omitted with 10% probability. This meant the underlying states were now only partially observable; for example, in Task 2 an odor signaled a transition to the ISI state with 90% probability.

To formalize these tasks, we largely followed previous work [7, 13]. Each task was modeled as a discrete-time Markov process with states $s_t \in \{1, \ldots, K\}$, where each t denotes a 200ms time bin (Fig 2A). These K "micro" states can be partitioned into those belonging to one of two "macro" states (corresponding to the ITI and the ISI; see Materials and methods). At each point in time, the agent's observation is one of $o_t \in \{odor, reward, null\}$ (Fig 2B). For each task, we trained the Belief model, and multiple Value RNNs ($N = 12$, each initialized randomly), on a series of observations from that task to estimate value using TD learning (see Materials and methods). Each RNN was a gated-recurrent unit cell [23], or GRU, comprised of $H = 50$ hidden units. Before training, the Value RNN's representation consisted of transient responses to each observation (S1 Fig). After training, we evaluated each model on a sequence of new trials from the same task (Fig 2C).

To confirm that this approach could recapitulate previous results, we measured the RPEs of each trained model (Fig 2D), where the model RPEs are calculated using Eq (2). Previous work showed that dopamine activity depended on the reward time differently in the two tasks, with activity decreasing as a function of reward time in Task 1, but increasing as a function of reward time in Task 2 [7] (Fig 3A). As in previous work, we found that this pattern was also exhibited by the RPEs of the Belief model (Fig 3B). We found that the RPEs of the Value RNN exhibited the same pattern (Fig 3C). In particular, the Value RNN's RPEs became nearly identical to those of the Belief model after training (Fig 3D). We emphasize that the Value RNN
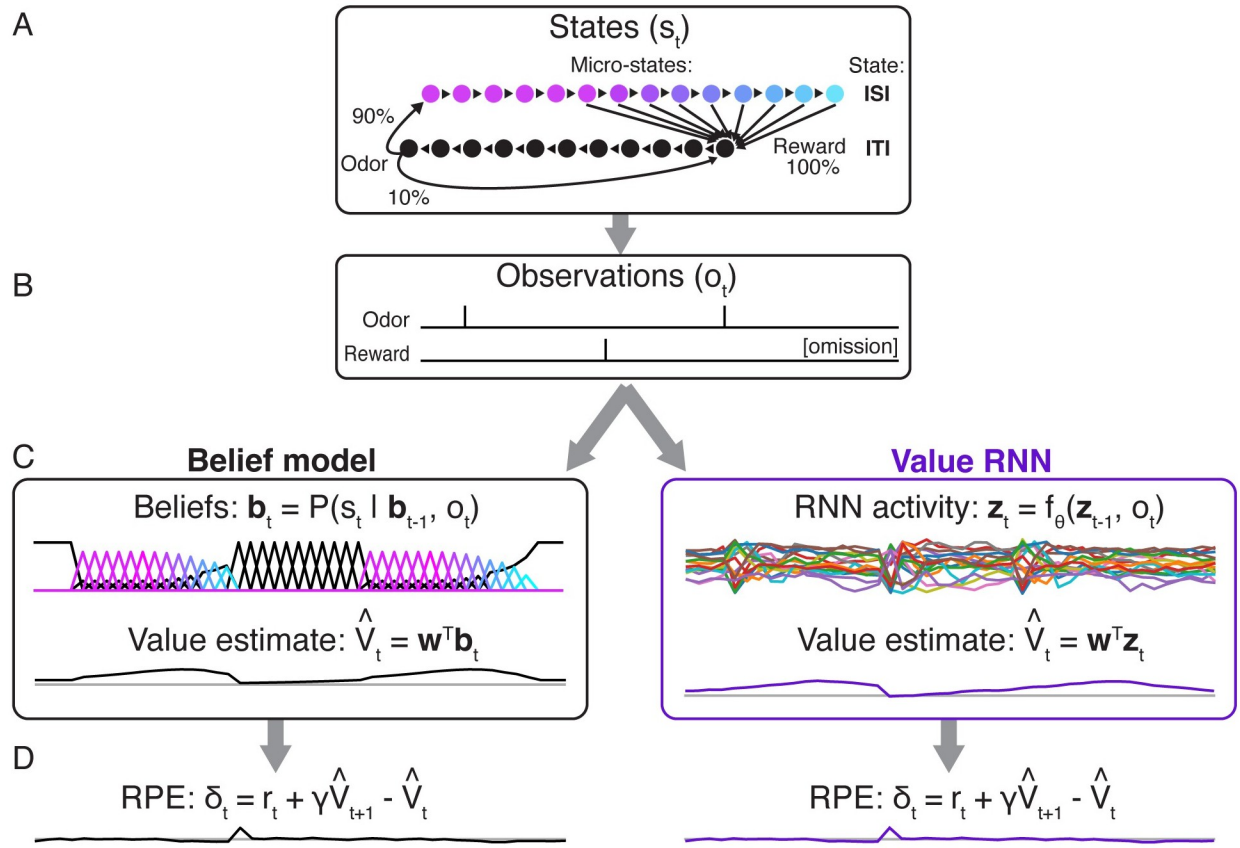
Fig 2. Observations, model representations, value estimates, and reward prediction errors (RPEs) during Task 2. A. State transitions and observation probabilities in Task 2. Each macro-state (ISI or ITI) is composed of micro-states denoting elapsed time; this allows for probabilistic reward times and minimum dwell times in the ISI and ITI, respectively. **B.** Observations emitted by Task 2 during two example trials. Note that omission trials are indicated only implicitly as the absence of a reward observation. **C.** Example representations (b_t, z_t) and value estimates ($\widehat{V}_t$) of two models (Belief model, left; Value RNN, right) for estimating value in partially observable environments, after training. **D.** After training, both models exhibit similar RPEs.

https://doi.org/10.1371/journal.pcbi.1011067.g002

was not trained to match the value estimate from the Belief model; rather, it was trained via TD learning using only observations. This result shows that, through training on observations alone, Value RNNs discovered a representation that was sufficient for both learning the value function as well as reproducing previously observed patterns in empirical dopamine activity.

We next asked whether the Value RNN learned to estimate value using representations that resembled beliefs. We considered three approaches to answering this question. First, we asked whether beliefs could be linearly decoded from the RNN's activity. Next, because beliefs are the optimal estimate of the true state in the task, we asked whether RNN activity could similarly be used to decode the true state. Finally, we took a dynamical systems perspective, and asked whether the RNN and beliefs had similar dynamical structure.

RNN activity readout was correlated with beliefs. We first asked whether there was a readout of the Value RNN's representation, z_t, that correlated with beliefs. Because the belief and RNN representations did not necessarily have the same dimensionality, we performed a multivariate linear regression to find the linear transformation of each RNN's activity that came closest to matching the beliefs (see Materials and methods). In other words, we found the linear transformation, $\widehat{W} \in \mathbb{R}^{K \times H}$, that could map each RNN's activity, $z_t \in \mathbb{R}^H$, to best
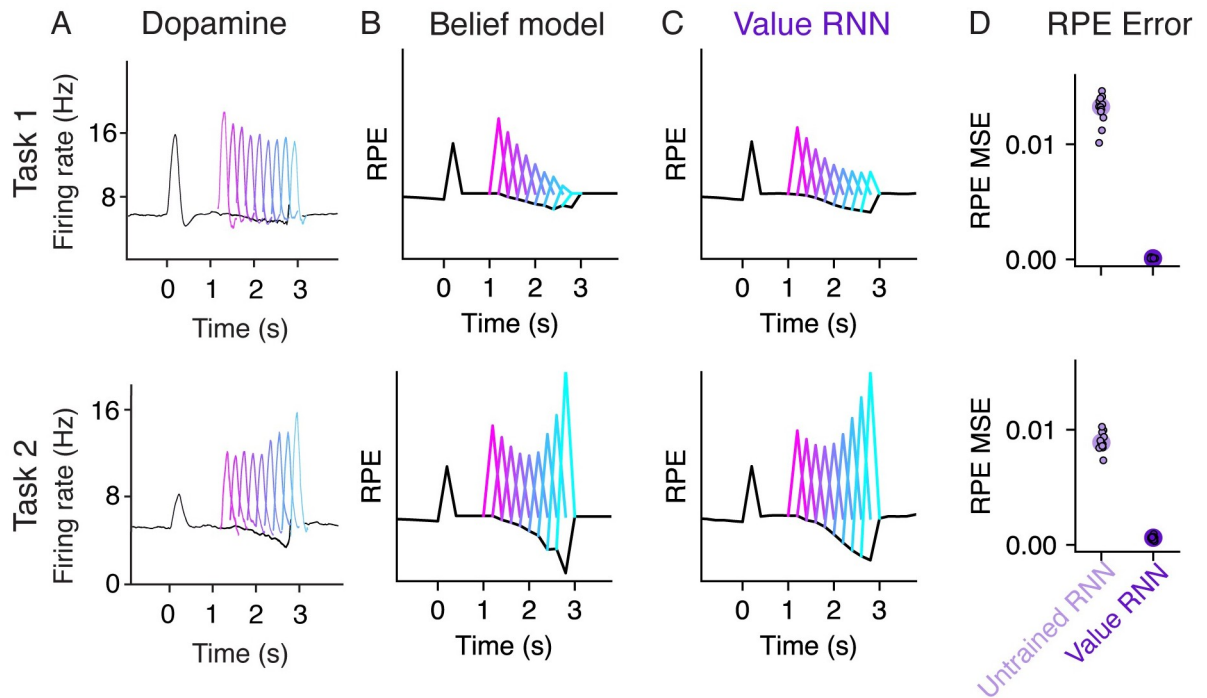
Fig 3. RPEs of the Value RNN resemble both mouse dopamine activity and the Belief model. A. Average phasic dopamine activity in the ventral tegmental area (VTA) recorded from mice trained in each task separately. Black traces indicate trial-averaged RPEs relative to an odor observed at time 0, prior to reward; colored traces indicate the RPEs following each of nine possible reward times. RPEs exhibit opposite dependence on reward time across tasks. Reproduced from Starkweather et al. (2017) [7]. **B-C.** Average RPEs of the Belief model and an example Value RNN, respectively. Same conventions as panel **A. D.** Mean squared error (MSE) between the RPEs of the Value RNN and Belief model, before and after training each Value RNN. Small dots depict the MSE of each of $N = 12$ Task 1 RNNs and $N = 12$ Task 2 RNNs, and circles depict the median across RNNs.

https://doi.org/10.1371/journal.pcbi.1011067.g003

match the belief vector, $\boldsymbol{b}_t \in \mathbb{R}^K$, across time:

$$\widehat{W} = \text{argmin}_W \sum_{t=1}^{T} \| W\boldsymbol{z}_t - \boldsymbol{b}_t \|_2^2$$

To quantify performance, we used held-out sessions to measure the total variance of the beliefs that were explained by the linear readout of RNN activity (R^2; see Materials and methods). We found that this readout of the Value RNN's activity explained most of the variance of beliefs (Fig 4B; Task 1 R^2: 0.61 ± 0.01, mean ± SE, $N = 12$; Task 2 R^2: 0.67 ± 0.02, mean ± SE, $N = 12$), substantially above the variance explained when using an RNN's activity before training (Task 1 R^2: 0.38 ± 0.01, mean ± SE, $N = 12$; Task 2 R^2: 0.41 ± 0.00, mean ± SE, $N = 12$). This is not a trivial result of the network's training objective, as the Value RNN's target (i.e., value) is only a 1-dimensional signal, whereas beliefs are a K-dimensional signal (here, $K = 25$). Nevertheless, we found that training a Value RNN to estimate value resulted in its representation becoming more belief-like, in the sense of encoding more information about beliefs.

RNN activity could be used to decode hidden states. The previous analysis assessed how much information about beliefs was encoded by the RNN's representation. Given that the belief representation is a probability estimate over all hidden states, we next asked whether the ground truth state could be decoded from the RNN's representation. To do this, we performed
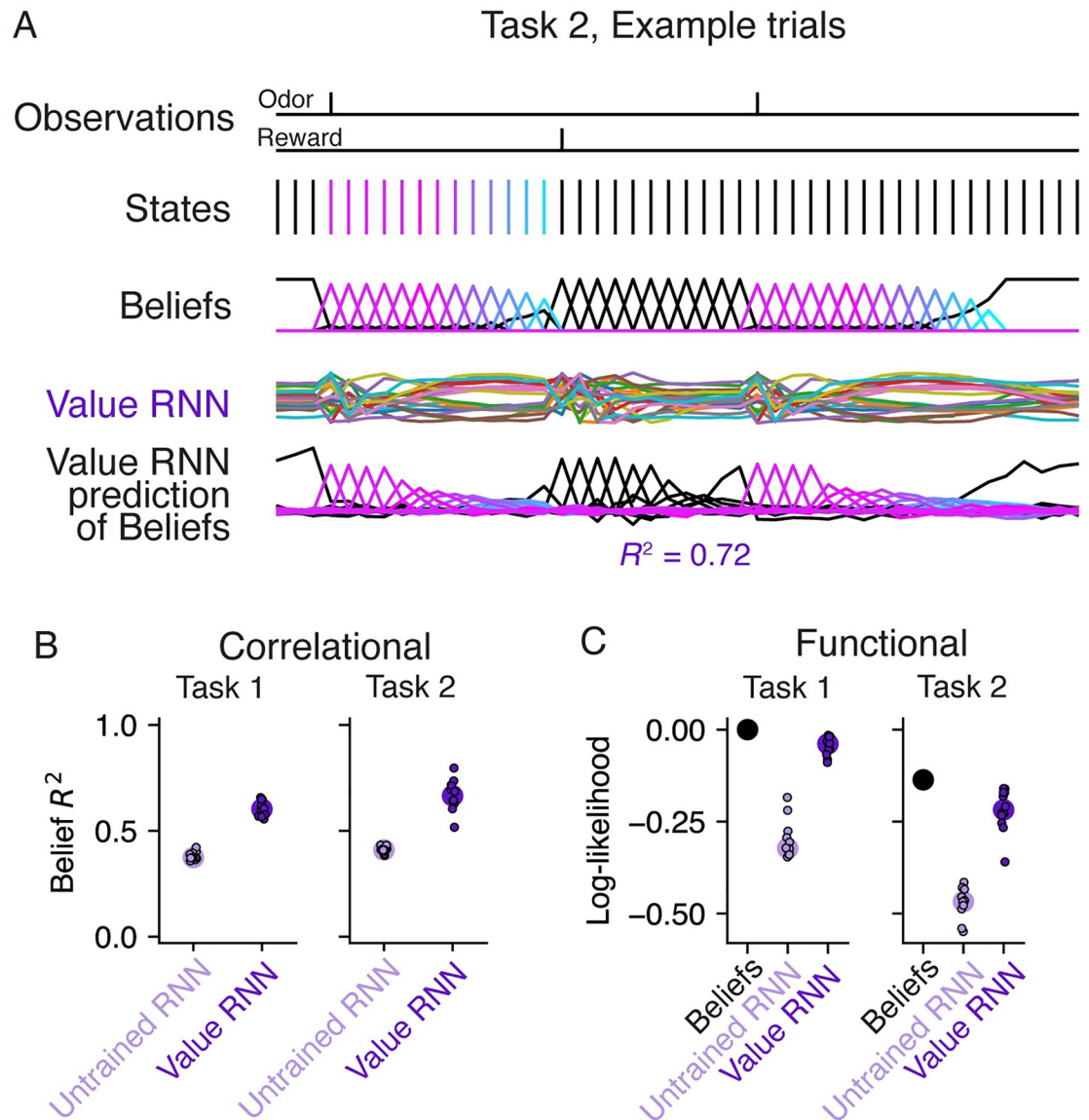
Fig 4. Value RNN activity readout was correlated with beliefs and could be used to decode hidden states. A. Example observations, states, beliefs, and Value RNN activity from the same Task 2 trials shown in Fig 2. States and beliefs are colored as in Fig 2, with black indicating ITI microstates, and other colors indicating ISI microstates. Note that the states following the second odor observation remain in the ITI (black) because the second trial is an omission trial. Bottom traces depict the linear transformation of the RNN activity that comes closest to matching the beliefs. Total variance explained (R^2) is calculated on held-out trials. **B.** Total variance of beliefs explained (R^2), on held-out trials, using different trained and untrained Value RNNs, in both tasks. Same conventions as Fig 3D. **C.** In purple, the cross-validated log-likelihood of linear decoders trained to estimate true states using RNN activity. Same conventions as Fig 3D. Black circle indicates the log-likelihood when using the beliefs as the decoded state estimate (i.e., no decoder is "trained").

https://doi.org/10.1371/journal.pcbi.1011067.g004

a multinomial logistic regression to find a linear transformation of each RNN's activity that maximized the log-likelihood of the true states (see Materials and methods). We quantified performance on held-out sessions by evaluating the log-likelihood of the decoded estimates. Because the beliefs capture the posterior distribution of the state given the observations under the true generative model, the log-likelihood of the beliefs is a ceiling on performance. We found that the log-likelihoods of the decoders trained on the RNNs' activity approached those

of the beliefs, and easily outperformed the decoders that used the activity of the RNNs before training (Fig 4C). Thus, training an RNN to estimate value resulted in a representation that could be used to more accurately decode the true state.

RNN activity exhibited belief-like dynamics.   One potential shortcoming of the above analyses is that we have not yet accounted for the dynamical nature of the belief representation: Belief updating can be thought of as a dynamical system describing how the posterior probability of each state evolves as a function of the observations. We therefore took a dynamical systems perspective [24–26] and asked whether the dynamics of the RNNs' representations resembled the dynamics of the beliefs in each task.

We first asked whether beliefs and RNNs had a similar fixed point structure, a standard approach to characterizing the computations performed by dynamical systems [24–26]. Here, by "fixed point" we mean a belief state that remains unchanged in the absence of observations (Fig 5A). In both tasks, the duration of the ITI is sampled from a geometric distribution, which has a constant hazard function. Thus, if the agent believes it is in the ITI (i.e., waiting for an odor), it should maintain this belief for as long as it receives no new observations ($\emptyset$). Thus, the ITI belief state is a fixed point of the belief updates in both tasks (Fig 5A). Now consider when the agent is in the ISI (e.g., following an odor observation). In Task 2 (Fig 5A, bottom panel), the agent should maintain a nonzero belief in the ISI only for as long as there are possible reward times remaining—i.e., the first 2.8s, or 14 time steps—but after that point it should return to the ITI state. Thus, the ITI state is the only fixed point of the Task 2 beliefs. In Task 1, by contrast, there are no omission trials, and so the beliefs are simply undefined when there are no observations for more than 14 time steps. Nevertheless, for the purposes of characterizing the fixed points of beliefs, we can ask what an agent with Task 1 beliefs *could* do when faced with an omission trial. In this sense, an agent could maintain a belief in the ISI for any number of time steps $X > 14$, resulting in two fixed points when $X \to \infty$, and one fixed point otherwise (Fig 5A, top panel). Thus, Task 1 beliefs can decay to the ITI fixed point at *any* point after 14 time steps, and may potentially have two fixed points.

We asked whether the Value RNNs in each task exhibited similar dynamics. To build intuition, we visualized the activity of an example Value RNN from each task (Fig 5B). To visualize the RNN's activity over time, $\boldsymbol{z}_t \in \mathbb{R}^{50}$, we used principal components analysis (PCA) to project the RNN's activity into the top two dimensions that captured the most variance of the activity across trials; the two dimensions shown in Fig 5B explained 83% and 79% of the total variance in the Task 1 and Task 2 Value RNN, respectively. We observed that each RNN's activity was quite stable during the ITI (purple circle), suggestive of a fixed point. An odor observation abruptly changed the RNN's activity (black vector), after which point the activity continued to move through state space during the ISI. On rewarded trials, in response to a reward (red vector), the RNN's activity gradually returned to the same ITI location it started from (purple circle). We noted that the activity of both RNNs would also have converged to its original ITI location had the reward been omitted (cyan traces). Interestingly, this was true even for the Task 1 RNN, which did not experience omission trials during training. These visualizations suggested that these two example Value RNNs had a single fixed point (corresponding to the ITI), which we confirmed numerically (see Materials and methods). We then used the same numerical approach to identify the fixed points across all trained Value RNNs, and found similar results. In fact, only two Value RNNs had more than one fixed point; these were both Task 1 RNNs, which had a fixed point for both the ITI and the ISI. Thus, the number of fixed points in the Value RNNs was consistent with the belief dynamics (as in Fig 5A).

Despite the fact that most Value RNNs had a single fixed point regardless of which task they were trained on, we noted that the temporal dynamics of RNN activity differed across the
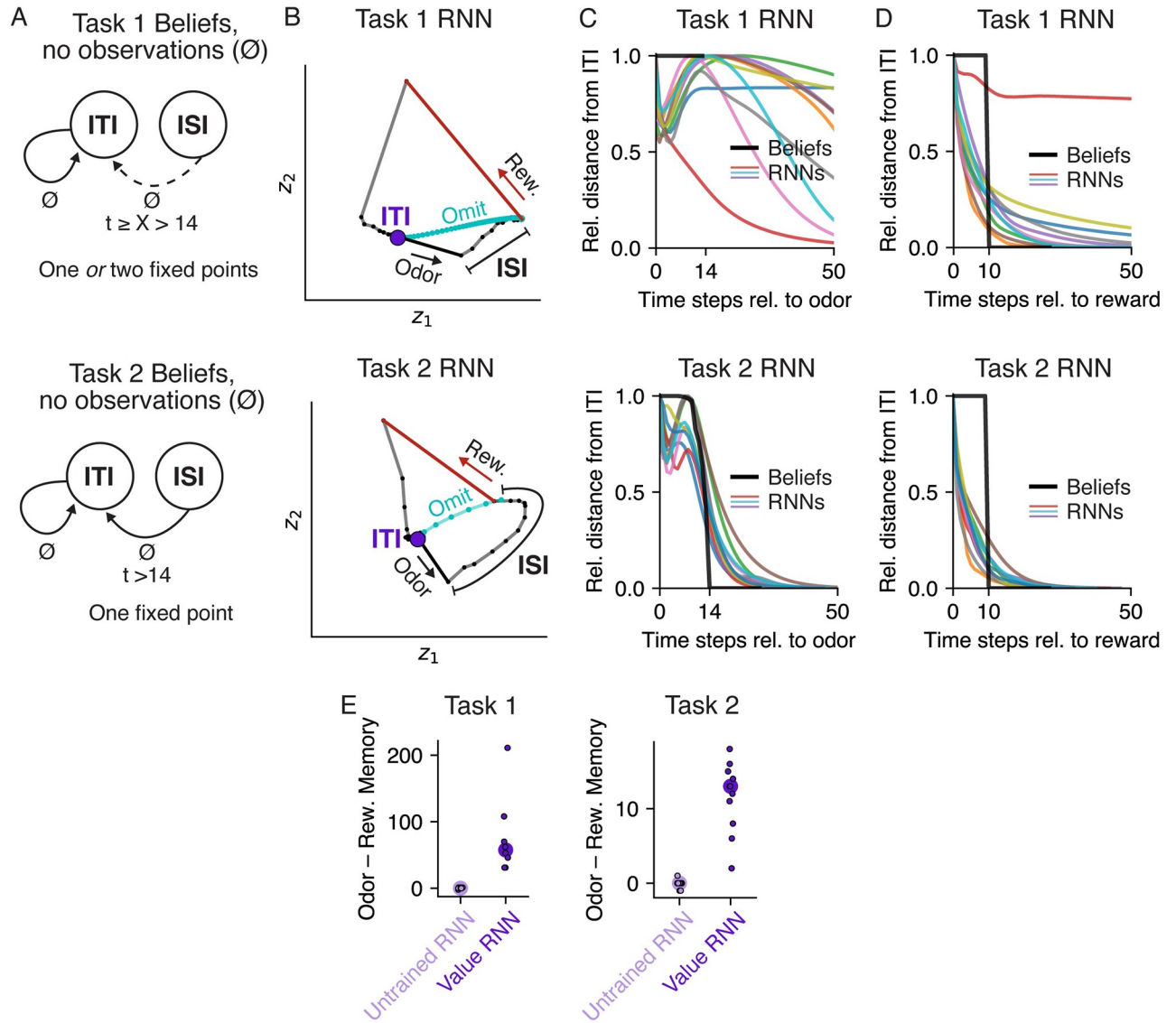
Fig 5. Value RNN dynamics resembled belief dynamics in each task. A. Dynamics of beliefs in Task 1 (top) and Task 2 (bottom). Black arrows indicate transitions between states in the absence of observations (∅) as a function of elapsed time, *t*, following an odor observation. 'X' indicates an unconstrained duration, and a dashed arrow indicates a transition that happens only when 'X' is finite. **B.** RNN activity at each time step (small black dots with connected lines) during an example trial in a 2D subspace identified using PCA, for two example networks trained on Task 1 (top) and Task 2 (bottom). Putative ITI fixed point indicated as purple circle. Vectors indicate the response to odor (black) and reward (red). Activity during an omission trial is shown in cyan, though note that omission trials were present in training data only for Task 2. **C-D.** Average normalized distance of each model's activity from its fixed point following an odor (panel **C**) or reward (panel **D**) observation, over time. To allow comparing distances across models, each model's distances were normalized by the maximum distance following each observation. **E.** Difference between each RNN's odor memory and reward memory, for Untrained RNNs and Value RNNs trained on each task. An RNN's odor memory is defined as the number of time steps after an odor that the RNN's activity returns to its ITI (see panel **C**); reward memory is defined similarly (see panel **D**). Same conventions as Fig 3D.

two tasks following odor observations. For example, in the Task 2 RNN, following an odor observation, the activity moved gradually closer to the ITI state throughout the ISI (Fig 5B, bottom subpanel). These dynamics allowed the Task 2 RNN's activity to return to the ITI state at the appropriate time on trials without reward (cyan trace). By contrast, in the Task 1 RNN, which did not experience trials without rewards during training, activity took much longer to

return to the ITI. To quantify these differences, we initialized each RNN to its fixed point, provided an odor observation, and then measured the RNN's activity over time in the absence of any subsequent reward. We then measured the distance of each RNN's activity over time from its ITI fixed point (Fig 5C, colored traces). We repeated this same analysis for beliefs (Fig 5C, black trace), allowing us to characterize the two models' responses to an odor as a function of the distance of their representations from their ITI fixed point. We reasoned that, if the RNNs learned belief-like dynamics, the activity of Task 2 RNNs should return to the ITI as soon as possible after time step 14 (i.e., the largest reward time), which we found was largely the case (Fig 5C, bottom subpanel). By contrast, in Task 1, there were no omission trials, and so the beliefs were undefined past time step 14. Thus, the activity of RNNs after time step 14 was not constrained by the task. Perhaps as a result of this, the Task 1 RNNs exhibited more variable decay rates (Fig 5C, top subpanel) relative to Task 2 RNNs. To quantify these differences across tasks, we calculated the number of time steps it took for a given RNN's activity to return to its ITI fixed point following an odor; we refer to this quantity as the RNN's *odor memory* (see Materials and methods). In fact, we found that *all* Task 1 RNNs had longer odor memories than every Task 2 RNN. Overall, these features were consistent with the beliefs in the two tasks following an odor observation: beliefs in Task 2, but not Task 1, must quickly return to the ITI after the maximum possible reward time. We also performed a similar analysis for reward observations, and refer to the time step at which an RNN's activity returned to the ITI fixed point following a reward the network's *reward memory*. Following a reward observation, the belief representation in both tasks returns to the ITI fixed point just after the minimum ITI duration (at time step 10), and we observed similar behavior in the trained RNNs (Fig 5D).

To summarize the presence of belief-like dynamics described above, we sought a single summary statistic to parallel those used to summarize the regression and decoding analyses in Fig 4. We noted that in both tasks, the belief representation's odor memory should be longer than its reward memory. This is because the odor memory is related to the maximum possible reward time (14 time steps after an odor), whereas the reward memory is related to the minimum ITI duration (10 time steps after a reward). To assess whether a given Value RNN exhibited this property, we computed the difference between its odor memory and reward memory as our summary statistic of that RNN's dynamics (i.e., *odor memory—reward memory*). We found that, in contrast to the untrained RNNs, *every* trained RNN in both tasks had an odor memory that was longer than its reward memory (Fig 5E). Thus, training an RNN to estimate value resulted in the RNN exhibiting belief-like dynamics, in terms of the network's memory for both odor and reward observations.

RNNs with larger capacity had more belief-like representations. Thus far, we have analyzed the representations of Value RNNs with the same number of hidden units ($H = 50$). To understand whether the network's size influences the types of representations learned, we next analyzed Value RNNs and Untrained RNNs with different numbers of hidden units.

We will first consider the Value RNNs. We found that Value RNNs with as few as 2 hidden units could learn the value function, as evidenced by their RPEs matching those of the Belief model (Fig 6A). In other words, despite there being 25 discrete states in our implementation of this task (and, as such, beliefs were 25-dimensional), an RNN with a 2-dimensional representation was sufficient to accurately estimate the value function. However, Value RNNs with fewer units had representations that were notably less belief-like, in terms of how well they could linearly encode beliefs (Fig 6B) and decode the true state (Fig 6C). This illustrates that learning a belief-like representation was not *necessary* for estimating the value function. Rather, the RNNs' representations were fully belief-like only when they had a sufficient number of hidden units.

As expected, the Untrained RNNs performed less well across the board, in terms of both their ability to match the Belief model's RPEs (Fig 6A), as well as their resemblance to the belief
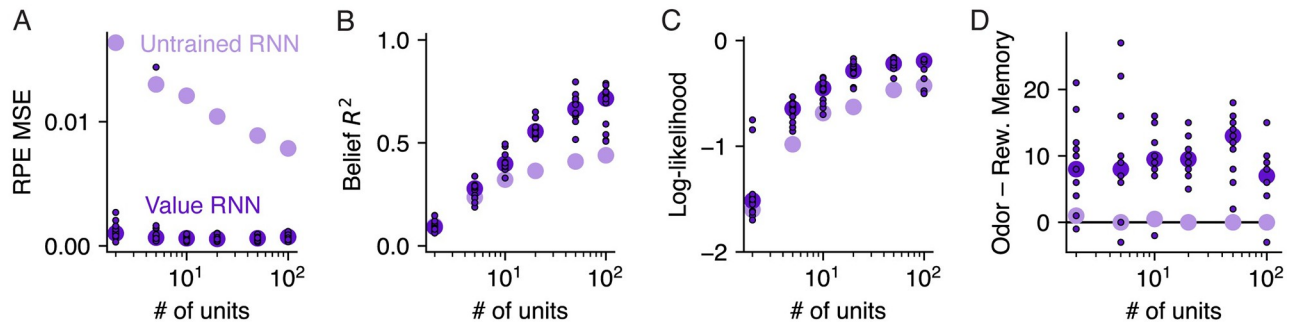
Fig 6. Value RNNs with larger capacity had more belief-like representations. A. Error between the RPEs of the Value RNN and Untrained RNN relative to the RPEs of the Belief model ("RPE MSE"; see Fig 3D) during Task 2, as a function of the number of units in the RNN. Each dot indicates the error for a single Value RNN. Circles indicate the median across the $N = 12$ Value RNNs (dark purple) and $N = 12$ Untrained RNNs (light purple) with the same number of units. Remaining panels use the same conventions. **B.** Total variance explained (R^2) of beliefs on held-out trials (see Fig 4B). **C.** Cross-validated log-likelihood of the state decoder using each RNN's activity to estimate the true state (see Fig 4C). **D.** Difference between each RNN's odor memory and reward memory (see Fig 5E).

representation (Fig 6B–6D). Nevertheless, we found that the Untrained RNNs' performance improved as a function of the number of units in many respects (Fig 6A–6C). While this is perhaps unintuitive, this was possible for the following reason: In the Untrained RNN model, though the RNN's *representation* was not learned, the value readout (used in Fig 6A), belief readout (Fig 6B), and state decoder (Fig 6C) were all fit to the training data (see Materials and methods). As we will discuss later in more detail (see subsection titled "Untrained RNNs could also be used to estimate value and encode beliefs"), this is an expected outcome from the perspective of "echo state networks" [27], where it is known that even randomly initialized RNNs can be paired with a learned readout to match any target signal, provided the RNN has enough units.

However, in contrast to the regression and decoding statistics, we observed that the dynamics-inspired statistic—the difference between a network's odor and reward memory—was belief-like (i.e., positive) only for Value RNNs, and across the full range of different numbers of hidden units (Fig 6D). This suggests that the dynamics perspective may be a more robust indicator of a network having a task-specific representation, as it most reliably distinguished between the trained and untrained RNNs.

Generalization to other tasks

We showed that RNNs could be trained to estimate value in the tasks from Starkweather et al. (2017) [7], and that the representations of these RNNs became more belief-like as a result of training. We next assessed whether the same basic insights generalized to a different task, that of Babayan et al. (2018) [10]. In this task, similar to Task 1 of Starkweather et al. (2017) [7], each trial consisted of an odor followed by a deterministic reward. Unlike in the Starkweather task, in this task the reward quantity on each trial was varied in blocks. In Block 1, each trial consisted of a small (1 μL) reward, while in Block 2 each trial consisted of a large (10 μL) reward. As a result, we formalize the states in this task using pairs of ITI and ISI states, one for each block (

Fig 7A). Importantly, the block identity was hidden to the animal, and was resampled uniformly every five trials. This meant that animals had to use the reward observations to infer which block they were currently in.

Previous work showed that the dopamine activity of animals trained on this task depended on the number of trials in the current block (Fig 7C), similar to what you would expect if animals used a belief representation (Fig 7D, dashed lines) [10]. To see if the Value RNN could reproduce these results, we trained $N = 12$ Value RNNs on this task. We found that Value RNNs exhibited nearly identical RPEs as the Belief model (Fig 7D). This was even true on probe sessions that included blocks with intermediate reward sizes, a setting in which both dopamine activity and belief RPEs exhibited a characteristic nonlinear relationship with reward size (S2 Fig). These results indicate that the Value RNNs found a representation sufficient for estimating value despite the hidden states.
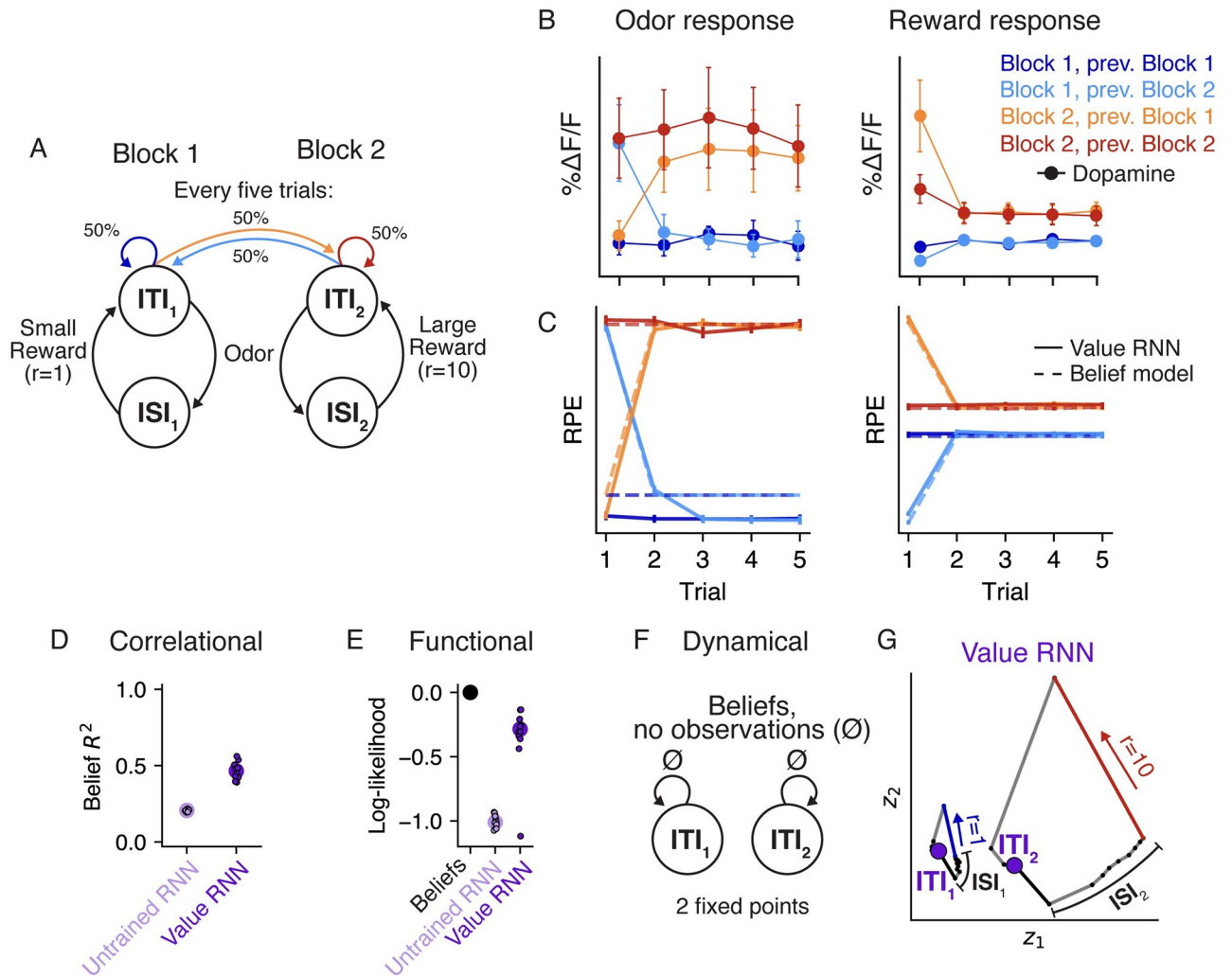

Fig 7. Value RNNs trained on Babayan et al. (2018) [10] reproduce Belief RPEs and learn belief-like representations. A. Task environment of Babayan et al. (2018) [10]. Each trial consists of an odor and a subsequent reward. The reward amount depends on the block identity, which is resampled uniformly every five trials. **B.** Average phasic dopamine activity in the VTA of mice trained on the task at the time of odor (left) and reward (right) delivery. Activity is shown separately as a function of the trial index within the block (x-axis) and the current/previous block identity (colors). Reproduced from Babayan et al. (2018) [10]. **C.** Average RPEs of the Belief model (dashed lines) and an example Value RNN (solid lines). Same conventions as panel **B**. **D.** Total variance of beliefs explained (R^2) using a linear transformation of model activity. Same conventions as Fig 4B. **E.** Cross-validated log-likelihood of linear decoders trained to estimate true states using RNN activity. Same conventions as Fig 4C. **F.** Dynamics of beliefs in the absence of observations. Same conventions as Fig 5A. **G.** Trajectories of an example Value RNN's activity, in the 2D subspace identified using PCA, during an example trial from Block 1 (left) and Block 2 (right). These two dimensions explained 68% of the total variance in the Value RNN's activity across trials. Putative ITI states indicated as purple circles. Same conventions as Fig 5B.

https://doi.org/10.1371/journal.pcbi.1011067.g007

We next asked whether, as in the Starkweather task, the Value RNN's representations resembled beliefs. To do this, we repeated the analyses in Fig 4. We found that the Value RNN's activity could be linearly transformed to match the beliefs (Fig 7D), and that its activity could also be used to decode the hidden states in the task (Fig 7E), as compared to RNNs not trained on the task. We next took a dynamical systems approach, characterizing the fixed points of beliefs in this task. Similar to Task 1 of Starkweather et al. (2017) [7] (Fig 5A), beliefs in the present task should have a fixed point at the ITIs for Block 1 and Block 2 (Fig 7F). To assess whether this was the case in the Value RNN, we visualized an example RNN's activity on the last few trials of each block, when the network should be confident as to the current block's identity (given the reward observations on previous trials). During these trials, we observed two non-overlapping trajectories of activity for each block (Fig 7G). Following a reward observation, the RNN's activity converged to a distinct location in state space corresponding to that block's ITI. This suggested the RNN had two fixed points, as in the belief representation. In reality, these were not both truly fixed points, as the RNN's activity did eventually return to a single fixed point given enough time without an observation (S3 Fig). However, the RNN's two putative ITI states remained distinct across the range of ITI durations present in the training data (S3 Fig), allowing the network to keep these trajectories (and thus the states corresponding to each block) separate. These analyses suggest that Value RNNs trained on this task also exhibited belief-like representations.

Untrained RNNs could also be used to estimate value and encode beliefs.   In the sections above we analyzed Value RNNs, whose representations were trained through TD learning. Here we take an alternative approach, inspired by reservoir computing, and consider in more detail the representations of untrained RNNs. In reservoir computing, a static dynamical system, or "reservoir," is combined with a learned linear readout. Given an appropriately initialized reservoir (e.g., an RNN), this approach can be used to approximate any nonlinear function [28]. Inspired by this approach, we explored whether we could choose a random initialization of our RNNs such that it was only necessary to learn a linear weighting of the RNN's representation to form its value estimate (i.e., ϕ in Eq (7) was fixed throughout training). Because this model resembles an echo state network ("ESN"; a reservoir computer whose reservoir is an RNN [27]), we will refer to this model as a Value ESN.

To see if the Value ESN model could be used to estimate value in partially observable environments, we trained Value ESNs to estimate value during Starkweather Task 2, while varying the gain used to initialize each network. Each Value ESN's RNN was initialized by sampling the matrix of recurrent weights as a random orthogonal matrix scaled by a single gain parameter [29], an approach commonly used to initialize RNNs (see Materials and methods). The gain effectively modulated the duration of the network's transient response to inputs (Fig 8A and 8B). Importantly, during training with TD learning, only the model's value weights were modified.

We found that for a range of different gains, the resulting Value ESN could estimate value nearly as well as Value RNNs, and recapitulate the experimentally observed dopamine patterns (Fig 8C). As expected from results in reservoir computing [28], the Value ESN's representations could also be linearly transformed to match beliefs (Fig 8D) or to decode the true hidden state (Fig 8E). We emphasize that the Value ESN's representation was determined solely by its initialization; given an appropriate initialization, the Value ESN's representation could effectively act as a set of temporal basis functions, allowing the network to match any downstream target, including beliefs. This result, alongside what we observed previously for Untrained RNNs with different numbers of hidden units (Fig 6B and 6C), underscores the fact that beliefs can be read out even from systems whose representations are not specific to the task at hand.

On the other hand, the Value ESN's representations differed substantially from those of the beliefs in terms of its dynamics: Among the best performing Value ESNs (i.e., those with a gain
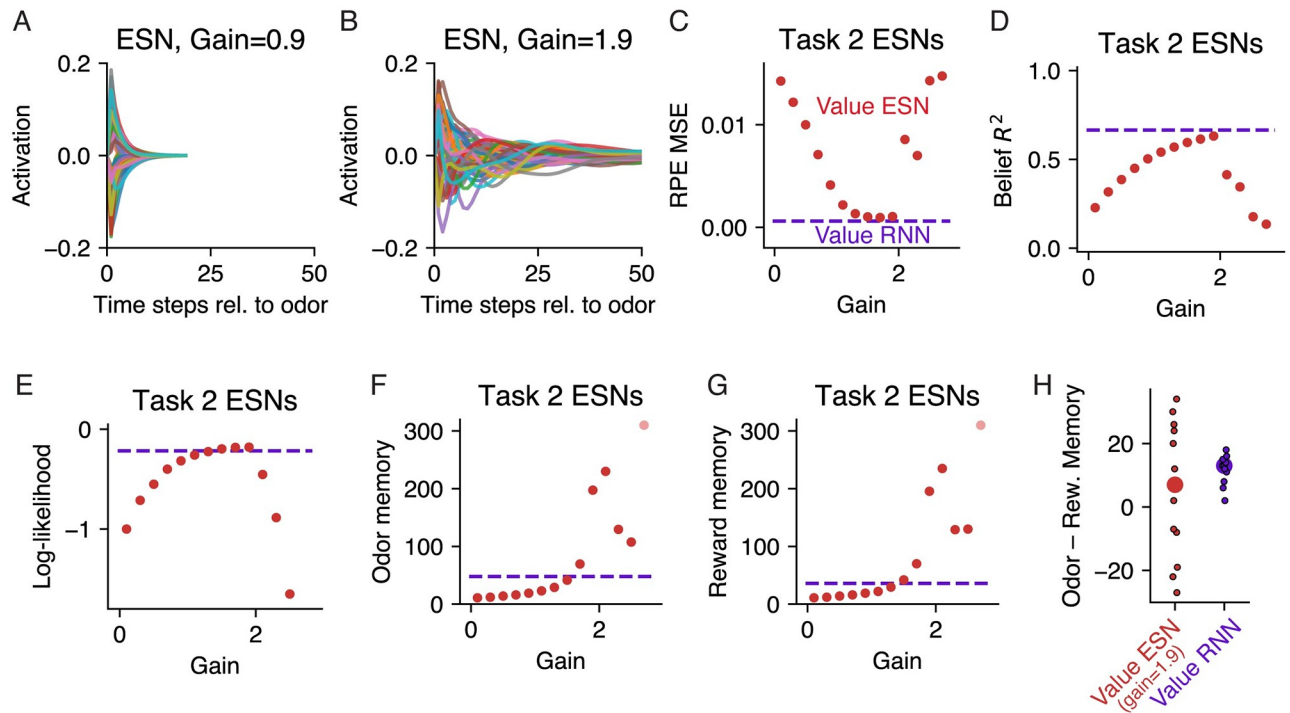
Fig 8. Untrained RNNs can be used to estimate value, read out beliefs, or decode hidden states, but do not resemble belief dynamics. A. Time-varying activations of 20 example units in response to an odor input, in an untrained RNN with 50 units, initialized with a gain of 0.9 (see Materials and methods). **B.** Same as panel **A**, but for an initialization gain of 1.9. **C.** RPE MSE (see Fig 3D) as a function of initialization gain, after training each Value ESN's value weights to estimate value during Starkweather Task 2. Circles depict the median across $N = 12$ Value ESNs initialized with the same gain. Dashed line indicates median across Task 2 Value RNNs with the same number of units. Same conventions for panels **D-G**. **D.** Belief R^2 (see Fig 4B) as a function of initialization gain. **E.** Cross-validated log-likelihood of state decoders (see Fig 4C) as a function of initialization gain. **F-G.** Number of time steps it took each Value ESN's activity to return to its fixed point following an odor (panel **F**) or reward (panel **G**) observation, as a function of the initialization gain. **H.** Difference between each model's odor memory and reward memory (see Fig 5E), for Value ESNs initialized with a gain of 1.9 (red) and Value RNNs (purple); same conventions as Fig 3D.

https://doi.org/10.1371/journal.pcbi.1011067.g008

of 1.9), following an odor observation, the Value ESN's activity returned to its fixed point after around 200 time steps ("odor memory"; Fig 8F), whereas Task 2 beliefs return to the ITI point after 15 time steps. The Value ESN's dynamics were nearly identical following a reward observation ("reward memory"; Fig 8G), such that, on average, the Value ESNs with a gain of 1.9 had no difference in their memory for odors versus rewards (Fig 8H). This is in striking contrast to the Value RNNs, each of which had an odor memory that was longer than its reward memory, in agreement with the belief dynamics. This difference is consistent with what we saw for Value RNNs versus Untrained RNNs with different numbers of hidden units (Fig 6D), where only the dynamical systems perspective indicated whether or not a network's representations had been trained on the task at hand. In sum, these results show that random RNNs can estimate value in partially observable environments, and even be used to read out beliefs and decode hidden states, provided they are carefully initialized. Nevertheless, only those networks whose representations were modified during training (i.e., the Value RNNs) exhibited dynamical responses consistent with those of a belief representation.

Discussion

We have shown that training RNNs to estimate value in partially observable environments yields representations that resemble beliefs. Specifically, we showed that, after training, an

RNN's activity i) could be linearly transformed to approximate beliefs, ii) could be used to decode the true state in the environment, and iii) had a dynamical structure consistent with beliefs. Importantly, we showed that the former two properties were also true of random, but properly initialized, RNNs. This illustrates that RNNs can generically exhibit many signatures of a belief representation, even if those representations are not specific to the task. On the other hand, we found that only the RNNs whose representations were modified during training exhibited belief-like *dynamical* signatures. Finally, we found that the representations of trained RNNs were most belief-like when they had a sufficient number of hidden units. These results indicate the importance of a multi-pronged approach in characterizing a system's representations.

Previous work at the intersection of neuroscience and machine learning has shown how agents performing reinforcement learning can use RNNs to solve a variety of tasks featuring state and task uncertainty, including tasks involving motor control [30], navigation [31–33], foraging [34], and decision-making [35, 36]. Our results, building on previous work [32, 34, 37], illustrate why RNNs offer an advantage in these settings: From a theoretical perspective, using an RNN resolves the problem of how to compute belief states, by replacing the fine-tuned Bayesian machinery needed for beliefs with a more general learned function approximator (e.g., a recurrent neural network) [32, 34, 37]. Our results illustrate that it is not necessary for an agent or animal to explicitly estimate states in partially observable environments using a belief representation; rather, agents can learn a sufficient representation for solving the task from observations alone. This is promising from a normative perspective, as it shows how neural circuits might come to compute theoretical features such as beliefs without that objective needing to be explicitly learned. Moreover, there is a growing toolkit for reverse engineering RNN solutions [25, 26, 38], which can shed light on learned mechanisms of value computation.

In this study, we considered classical conditioning tasks where previous studies had suggested that dopamine activity reflected a belief representation [6–11]. These tasks were a convenient setting to study the emergence of belief representations in RNNs for two reasons. First, these tasks had relatively simple state spaces and dynamics. This allowed us to calculate the true beliefs in closed-form, and thereby directly compare the beliefs to the representations learned by the RNNs. The simplified nature of the tasks also allowed us to consider RNNs with a small number of units, simplifying both training and analysis. Second, in these tasks, the agent's actions do not impact the trial structure (i.e., the sequence of observations and rewards), which means that both the value function and the beliefs are independent of the agent's actions. In this setting, the value function is a linear function of the beliefs, whereas in a general partially observable environment, the value function also depends on the agent's action policy. This allowed us to compare how different models (e.g., the Belief model and the Value RNN) solved the value estimation problem without having to also consider the action policy. An important direction for future work is to extend our analyses to tasks with larger state spaces, and to tasks where the agent's policy influences the visited states. One possibility is that, in these settings, an agent's policy will influence the degree to which the learned representations resemble beliefs. For example, if the agent's policy only explores a limited region of the total state space, it may be difficult for the agent to acquire beliefs about the less explored regions of state space.

One potential benefit of the Value RNN over the Belief model for estimating value is the ability to separate the capacity of the model (i.e., the number of hidden units in the RNN) from the size of the state space in the environment. As we showed in Fig 6, Value RNNs with fewer units had representations that were not linearly transformable into beliefs (Fig 6B), but these networks were nevertheless able to estimate the value function (Fig 6A). Value RNNs

with more units had more belief-like representations. This suggests a potentially useful trade-off, in which agents could choose to allocate more capacity to a task in exchange for more belief-like representations. Such a trade-off may be a relevant feature for biological organisms, who must be able to perform tasks such as value estimation in complex environments where it may not always be feasible to learn the full belief representation.

From a methodological perspective, this work can serve as a blueprint for how to bridge analyses of neural computation across levels of abstraction. In future work, we hope to apply this framework to test neural models of how animals perform associative learning via reinforcement learning. For instance, previous work has suggested that prefrontal cortex may perform state estimation in tasks with hidden states [6, 7, 12, 13]. The same tools we apply here to artificial neural networks can also be applied to neural activity recorded from animals performing the same task. For instance, if cortex implements something like a Value RNN, cortical activity may show a longer transient response to odors in Task 1 versus Task 2 (Fig 5C), or a longer transient response to odors than to rewards (Fig 5E). On the other hand, if activity is more like a Value ESN, cortical dynamics may be largely the same across different tasks, and in response to different observations.

Previous work has shown that, in animals, prefrontal cortex activity is a necessary component of animals' state representations [13]. This work found that inactivating prefrontal cortex in the Starkweather task led to animals' RPEs in Task 2 resembling the RPEs of Task 1. This is what one would expect if prefrontal cortex was involved in estimating a belief in omission trials. In fact, both Tasks 1 and 2 include another form of uncertainty, which is the reward time on each trial. The fact that prefrontal inactivation did *not* interact with animals' estimates of timing suggests that different neural circuits may form belief-like representations specific to particular types of state uncertainty (e.g., temporal uncertainty versus reward uncertainty). In the present work, our RNNs should be thought of as a generic computational model, and not a model of individual brain regions. These networks had a generic architecture and only a single layer; as a result, our model would be unable to distinguish between different sources of uncertainty. Nevertheless, it is an interesting question how architectural considerations, such as layer connectivity and the dominance of feedforward versus recurrent connectivity, might contribute to where in the brain different belief-like representations are formed.

Traditional models of how animals perform trace conditioning tasks like the ones we consider here make a variety of implicit assumptions about how animals represent the passage of time [39, 40]. For example, the state space shown in Fig 2A, which forms the basis of the belief representation, conceptualizes the passage of time in the form of microstates. Many modeling efforts require even more assumptions to account for scalar variability in animals' estimates of elapsed time, such as by incorporating a more complex set of temporal basis functions. In our model, by contrast, the Value RNN's time-varying representation of inputs is learned through training. We observed that individual units in our RNNs were tuned to elapsed time relative to observations, and that the temporal precision of tuning decreased with elapsed time (S1 Fig), both of which are standard assumptions of microstate representations [41]. Similarly tuned "time cells" have been observed in the striatum [42], hippocampus [43], and prefrontal cortex [44]. Our modeling suggests that at least some assumptions about microstate representations may be redundant in the sense that they may emerge naturally in recurrent networks that are trained to perform reinforcement learning. This viewpoint resonates with the idea (reviewed in [45]) that delay encoding can arise as an emergent property of neural network dynamics.

Our results show that computing beliefs explicitly is not a necessary precursor for optimally performing a task in partially observable environments. Nor is it required to reproduce experimentally observed patterns of dopamine neuron activity. Instead, our results show that

training a nonlinear function approximator (such as an RNN) using TD learning results in a representation sufficient for estimating value in partially observable environments. An interesting question for future work is whether other training objectives, such as predicting the next observation [46], might yield similar results. What advantage, if any, might an explicit belief representation confer to an agent? Beliefs are an efficient representation in that they are sufficient for solving *any* task in the same environment. Thus, beliefs may be a desirable representation for animals, who may need to achieve a range of different goals in the same environment (e.g., finding water when thirsty, but finding food when hungry) without having to learn a representation in each of these tasks separately. Future work should explore whether a dedicated belief mechanism is necessary in these multi-task settings, or if the RNN framework we present here can also yield representations that effectively generalize to new tasks in the same environment.

Materials and methods

Task implementation

In each experiment, at each time step t, agents received two observations: an odor cue, $c_t \in \{0, 1\}$; and a reward, $r_t \in \{0, r\}$, where $r > 0$ depended on the task (see below). We will refer to the total observation vector as $\boldsymbol{o}_t = [c_t, r_t]$. We treated each time step as equal to 200ms.

Each trial began with an intertrial interval (ITI), $t_{ITI} \in \mathbb{N}$, during which there were no observations ($\boldsymbol{o}_t = 0$ for $t < t_{ITI}$). The ITI (offset by a minimum delay of 10 time steps) was sampled as $t_{ITI} - 10 \sim \text{Geom}\left(p_{ITI} = \frac{1}{8}\right)$, where $\text{Geom}(p)$ is a geometric distribution with parameter p.

Following the ITI, a single odor cue was presented as $c_t = 1$ for $t = t_{ITI}$. The cue was then followed by another interval with no observations, called the interstimulus interval (ISI), $t_{ISI} \in \mathbb{N}$. A reward was then presented as $r_t > 0$ for $t = t_{ITI} + t_{ISI}$, after which point the trial terminated. The details of the ISI and reward size depended on the specific task, as described below.

Starkweather tasks. There were two versions of this task. In both Tasks 1 and 2, every non-zero reward size had $r_t = 1$. In Task 2, with probability $p_{omission} = 0.1$, the reward on a given trial was omitted, such that $r_t = 0$ for the duration of the trial. In both tasks, the ISIs on each trial were sampled from a discretized Gaussian with mean $\mu = 10$, standard deviation $\sigma = 2.5$, and range $6 \leq t_{ISI} \leq 14$, as in Starkweather et al. (2017) [7].

Babayan task. In this task, non-zero reward sizes were determined in blocks of trials. In block 1, the non-zero reward size was $r_t = 1$, while in block 2 the non-zero reward size was $r_t = 10$. Each block consisted of 5 sequential trials. Block identities were sampled uniformly with equal probability. On all trials, the ISIs were uniformly sampled as $t_{ISI} \sim \text{Unif}(\{9, 10, 11\})$. For S2 Fig, sessions also included blocks of intermediate rewards: $r_t \in \{1, 2, 4, 6, 8, 10\}$, where block identities were sampled in similar proportions to those used in Babayan et al. (2018) [10] (i.e., blocks with $r_t = 1$ or $r_t = 10$ comprised ∼90% of the total trials).

Recurrent neural network implementation

We trained recurrent network models, in PyTorch, on multiple tasks to estimate value. Each *Value RNN* consisted of a GRU cell [23] with $H \in \mathbb{N}$ units, followed by a linear readout of value. At each time step t, the RNN received observations, $\boldsymbol{o}_t \in \mathbb{R}^2$, from a given experiment. The RNN's representation can be written as $\boldsymbol{z}_t = f_{\boldsymbol{\phi}}(\boldsymbol{z}_{t-1}, \boldsymbol{o}_t)$ given parameters $\boldsymbol{\phi}$. The RNN's output was the value estimate $\widehat{V}_t = \boldsymbol{w}^\top \boldsymbol{z}_t + w_0$, for $\boldsymbol{w} \in \mathbb{R}^H$ and $w_0 \in \mathbb{R}$. The full parameter vector $\boldsymbol{\theta} = [\boldsymbol{\phi}, \boldsymbol{w}, w_0]$ was learned using TD learning. This involved backpropagating the

gradient of the squared error loss $\delta_t^2 = (r_t + \gamma \widehat{V}_{t+1} - \widehat{V}_t)^2$ with respect to $\widehat{V}_t$. Unless otherwise noted we used $\gamma = 0.93$ as in Starkweather et al. (2018) [13].

RNNs were trained on episodes composed of 20 (Starkweather task) or 50 (Babayan task) concatenated trials. This was necessary to allow models to accurately estimate the value of the ITI, but it also meant that episodes included long gaps of time without any inputs. We used a GRU cell rather than a simple Elman (i.e., gate-less) recurrent network as we found the former easier to train to convergence. We suspect that the gate-less RNNs struggled to converge due to the vanishing gradient problem, which is a known issue with these networks in the presence of long time lags [47].

For each task, and for each $H \in \{2, 5, 10, 20, 50, 100\}$ units, we trained $N = 12$ networks. Prior to training each network, the weights and biases of the GRU (i.e., ϕ) were initialized using PyTorch's default of $\mathcal{U}(-a, a)$ where $a = \frac{1}{\sqrt{H}}$. Training then proceeded for a maximum of 150 epochs on a session of 10,000 trials, with a batch size of 12 episodes. Training was stopped early if the loss increased for 4 consecutive epochs. Gradient updates used Adam with an initial learning rate of 0.003. No hyperparameter search was performed to fine-tune these choices. In the text, we refer to a *Value RNN* as the result of this training process, while an *Untrained RNN* is the same network after initialization but before training.

The *Value ESN* was identical to the Value RNN, except that it was initialized differently, and ϕ was frozen during training (i.e., the only learned parameters were $\boldsymbol{w}$ and w_0). For initialization, we did the following ("Tensorflow-style" initialization). All of the GRU's biases were initialized to zero. The GRU's recurrent weights were sampled as a random orthogonal matrix using `torch.nn.init.orthogonal_` with a given gain [29]. The GRU's input weights were sampled as $\mathcal{U}(-a, a)$ where $a = \sqrt{\frac{6}{2+H}}$, using `torch.nn.init.xavier_uniform_` [48].

State and belief representations

Given a task with hidden states $s \in \{1, \ldots, K\}$, the belief, $\boldsymbol{b}_t \in [0, 1]^K$, is the posterior probability distribution over each possible state [17]. The tasks we analyze here are technically discrete-time semi-Markov processes, and so we follow previous work in formulating them equivalently as Markov processes with micro-states defined over each relevant discrete time step [6, 7]. In this setting, observations occur at the transition between states. As a result, the belief in state can be written as:

$$b_t(k) \propto \sum_{k'=1}^{K} O_{o_t}(k', k) T(k', k) b_{t-1}(k') \tag{10}$$

where $T \in [0, 1]^{K \times K}$ is the matrix of transition probabilities, and $O_o(k', k)$ is the probability of observing o after making a transition from k to k'.

Note that for a partially observable Markov process with a finite state space and no actions, the true value function can be written as a weighted combination of beliefs:

$$V_t = \sum_{k=1}^{K} V(k) b_t(k) \tag{11}$$

where $V(k)$ and $b_t(k)$ are the value and belief of state $s_t = k$, respectively. This means that the linear value function approximation in Eq (4) is sufficiently expressive for the partially observable problems we consider in this paper: with enough training data, a linear value function

approximation will perfectly estimate the true value function (i.e., given learned weights $w(k) = V(k)$ and features $z_t(k) = b_t(k)$ for each $k \in K$).

Starkweather tasks. In both Tasks 1 and 2 there are three distinct observations, $\boldsymbol{o}_t \in \{[0, 0], [1, 0], [0, x]\}$, which we refer to as the null, odor, and reward observations, respectively. Let the possible reward times be $t_{ISIs} = \{6, \ldots, 14\}$. The maximum reward time is $\max(t_{ISIs}) = 14$, and so we let states $1 - 14$ be the ISI microstates. The ITI is a Geometric distribution plus a minimum ITI of $t_{ITI} = 10$, and so we let states $15 - 25$ be the ITI microstates. There are $K = 25$ total states.

We first define the observation probabilities, $O_{null}, O_{odor}, O_{reward} \in \{0, 1\}^{K \times K}$, where $O_o(k', k)$ indicates the probability of having transitioned from state k to state k' upon observing $o \in \{null, odor, reward\}$. Each $O_o(k', k) = 0$ except at the following:

- $O_{null}(t + 1, t) = 1$ for all $t \neq \max(t_{ISIs})$

- $O_{null}(K, K) = 1$

- $O_{odor}(t, K) = 1$ for $t = 1$ (Task 1) or $t \in \{1, \max(t_{ISIs}) + 1\}$ (Task 2)

- $O_{reward}(\max(t_{ISIs}) + 1, t) = 1$ for $t \in t_{ISIs}$

To define the transition probabilities, let $p_t \in [0, 1]$ be the probability of receiving reward at time $t \in t_{ISIs}$, $F_t = \sum_{t' \leq t} p_{t'}$ the cumulative probability, and $h_t = p_t/(1 - F_t)$ the hazard. Recall that $p_{ITI} = \frac{1}{8}$. Then $T(k', k) = 0$ except at the following:

- $T(t + 1, t) = 1$ for $t \notin \max(t_{ISIs})$

- $T(t + 1, t) = 1 - h_t$ and $T(\max(t_{ISIs}) + 1, t) = h_t$ for $t \in t_{ISIs}$

- $T(K, K) = 1 - p_{ITI}$

- $T(\max(t_{ISIs}) + 1, K) = p_{ITI} p_{omission}$

- $T(1, K) = p_{ITI}(1 - p_{omission})$

Babayan task. The states in this task can be thought of as two copies of the beliefs in the Starkweather tasks, with one copy for each of the two blocks. (Note that $t_{ISIs} = \{9, 10, 11\}$, $K = 22$, and the hazard probabilities must be modified from the Starkweather task to account for the different reward timing distribution). Each copy has 11 ISI microstates (because the maximum reward time is $\max(t_{ISIs}) = 11$) and 11 ITI microstates. Let $\boldsymbol{b}_t^{(1)} \in [0, 1]^{22}$ and $\boldsymbol{b}_t^{(2)} \in [0, 1]^{22}$ be the beliefs for the substates of block 1 and block 2, respectively. Let the notation $\boldsymbol{x} = [\boldsymbol{y}, \boldsymbol{z}]$ indicate that $\boldsymbol{x} \in \mathbb{R}^{K_1 + K_2}$ is a concatenation of the vectors $\boldsymbol{y} \in \mathbb{R}^{K_1}$ and $\boldsymbol{z} \in \mathbb{R}^{K_2}$. Then the full belief $\boldsymbol{b}_t \in [0, 1]^{44}$ is as follows:

$$
\begin{aligned}
\boldsymbol{b}_t &= [p_t \boldsymbol{b}_t^{(1)}, \quad (1 - p_t) \boldsymbol{b}_t^{(2)}] \\
p_t &= f(r_t) \text{ if } r_t > 0 \text{ otherwise } p_{t-1}
\end{aligned}
\tag{12}
$$

where $p_t \in [0, 1]$ is the estimated probability of being in block 1, and f is our likelihood function mapping nonzero rewards, r_t, to the estimated probability of being in block 1 vs. block 2. In other words, we modeled the belief in the block identity as being a function only of the most recently observed reward. We defined f following the original paper: Let $\phi(r_t; \mu, \sigma_r)$ be the pdf of a Normal distribution with mean μ and standard deviation $\sigma_r > 0$. Then $f(r_t) = \frac{\phi(r_t; \mu_1, \sigma_r)}{\phi(r_t; \mu_1, \sigma_r) + \phi(r_t; \mu_2, \sigma_r)}$, where $\mu_1 = 1$ and $\mu_2 = 10$ are the rewards amounts in block 1 and 2, respectively. Here we assumed σ_r was arbitrarily small, so we used $\sigma_r = 0.001$.

Model analyses

We analyzed exemplars from each model class (Beliefs, Value RNNs, Untrained RNNs, Value ESNs) using two sessions of 1,000 concatenated trials each, with the same task parameters as those used when training the RNNs (see above). The first session was used for fitting any parameters relevant to the analysis (i.e., value weights, regression weights, decoding weights), while the second session was used for evaluation. Because the RNN's responses were deterministic functions of their inputs, prior to analysis we added noise to all RNN representations to prevent overfitting during regression and decoding as follows. Let $\sigma_i > 0$ be the sample standard deviation of the activity of hidden unit i across trials, and let $g > 0$ be the noise gain. Then we added zero-mean Gaussian noise with a standard deviation of $g\sigma_i$ to this unit's activity, so that each unit had the same SNR, where SNR $= 10 \log_{10}(\sigma_i^2 / (\sigma_i^2 g^2))$ dB $= -20 \log_{10} g$ dB. For the figures in the main text, we used $g = 0.05$, such that SNR ≈ 26 dB. Our main conclusions did not change for other values of g (S4 Fig).

Value estimates. Each model's value estimate was given by $\widehat{V}_t = \boldsymbol{z}_t^\top \widehat{\boldsymbol{w}} + w_0$, where $\widehat{\boldsymbol{w}} \in \mathbb{R}^D$ and $w_0 \in \mathbb{R}$ are the value weights, and $\boldsymbol{z}_t \in \mathbb{R}^D$ is the model's representation at time t. (For the belief model, $\boldsymbol{z}_t = \boldsymbol{b}_t$).

To estimate the value weights, $\widehat{\boldsymbol{w}}$, we used Least-Squares TD (LSTD) [49]. LSTD provides a closed-form solution for the weights, $\widehat{\boldsymbol{w}}$, that minimizes the TD error, $\delta_t = r_t + \gamma \widehat{V}_{t+1} - \widehat{V}_t$, across all observed data as follows:

$$
\begin{aligned}
\widehat{\boldsymbol{w}} &= \widehat{D}^{-1}\widehat{\boldsymbol{d}} \\
\widehat{D} &= \sum_{t=1}^{T-1} \boldsymbol{z}_t (\boldsymbol{z}_t - \gamma \boldsymbol{z}_{t+1})^\top \\
\widehat{\boldsymbol{d}} &= \sum_{t=1}^{T-1} r_t \boldsymbol{z}_t
\end{aligned}
\tag{13}
$$

This procedure was used to fit value weights for all models considered in the paper: the Belief model, Value RNN, Untrained RNN, and Value ESN. Note that the Value RNN and Value ESN learned their own value weights, $\widehat{\boldsymbol{w}}$, as part of training. However, we wanted to ensure that the value functions of all models were estimated using the same procedure, so we re-estimated these models' value weights using LSTD after training.

Reward prediction errors. To assess how close each RNN's RPEs came to the RPEs found using the belief model, we defined an RNN's RPE error using the mean squared error: $\frac{1}{T}\sum_{t=1}^{T} (\delta_t - \widehat{\delta}_t)^2$, where $\widehat{\delta}_t$ is the RNN's RPE, and δ_t is the RPE from the belief model. Because each trial had at most one reward delivery, for simplicity we considered the RPEs only at the time of reward delivery on each trial (i.e., the t in the above equation refers to a trial and not a time step); this simplification did not affect our results.

Belief R^2. To assess how much variance of the beliefs could be explained by each model's learned representation, we used multivariate linear regression:

$$
\widehat{W} = (Z^\top Z)^{-1} Z^\top B
\tag{14}
$$

where $Z \in \mathbb{R}^{T \times (H+1)}$ is the matrix whose t^{th} row is $[\boldsymbol{z}_t, 1]$, $B \in \mathbb{R}^{T \times K}$ is the matrix whose t^{th} row is $\boldsymbol{b}_t$, and $\widehat{W} \in \mathbb{R}^{(H+1) \times K}$. We considered linear (rather than nonlinear) regression to be conservative in our conclusions about the degree to which model representations resembled beliefs.

To evaluate model fit, let $\mathrm{Var}(X) = \frac{1}{T}\sum_{t=1}^{T} \| \boldsymbol{x}_t - \bar{\boldsymbol{x}} \|_2^2$, where $\mathbf{x}_t$ is the tth row of X, and $\bar{\boldsymbol{x}}$ is the mean of the rows of X. Then we calculated the total variance explained:

$$R^2 = 1 - \frac{\mathrm{Var}(B - Z\widehat{W})}{\mathrm{Var}(B)} \tag{15}$$

State decoding.   We asked where we could find a decoder that could infer the underlying state, $s_t \in \{1, \ldots, K\}$, using an affine transformation of the RNN's representation, $\boldsymbol{z}_t \in \mathbb{R}^H$. To find such a decoder, we first standardized each model representation (considering each dimension of $\boldsymbol{z}_t$ in isolation) to have zero mean and unit variance. We then performed a multinomial logistic regression using scikit-learn's `linear_model.LogisticRegression` with the parameters `multi_class="multinomial"`, $C = 1$, and `max_iter = 1e4`.

After training, the decoder's estimated state probabilities over s_t are:

$$\boldsymbol{\pi}_t = \mathrm{softmax}(\tilde{\boldsymbol{z}}_t^\top \widehat{W}) \in [0, 1]^K \tag{16}$$

where $\widehat{W} \in \mathbb{R}^{(H+1)\times K}$ contains the decoder parameters; $\tilde{\boldsymbol{z}}_t \in \mathbb{R}^{H+1}$ is the model representation at time t after standardization, plus an extra constant column of 1's to fit the offset; and the softmax function normalizes the vector to be a valid probability over the K values of s_t.

To evaluate the resulting decoder, we calculated the model's log-likelihood (ℓ) on the evaluation session as follows:

$$\ell(\widehat{W} \mid s_1, \ldots, s_T, \tilde{\boldsymbol{z}}_1, \ldots, \tilde{\boldsymbol{z}}_T) = \frac{1}{T}\sum_{t=1}^{T} \log(\boldsymbol{\pi}_t(s_t)) \tag{17}$$

where $\boldsymbol{\pi}_t(s_t) \in [0, 1]$ is the s_t^{th} entry of the vector $\boldsymbol{\pi}_t$. We calculated the log-likelihood for the belief model similarly, except instead of training a decoder we used $\boldsymbol{\pi}_t = \mathbf{b}_t$. For the Babayan task (Fig 5E), we calculated the log-likelihood on all trials except the first trial in each block. This was necessary for the beliefs to act as an upper-bound on the log-likelihood, because we defined the beliefs in a way that did not assume knowledge of the number of trials in each block.

Dynamics analysis.   An RNN with parameters $\boldsymbol{\phi}$ has a hidden state that evolves as $\boldsymbol{z}_t = f_{\boldsymbol{\phi}}(\boldsymbol{z}_{t-1}, \boldsymbol{o}_t)$. Conditioned on a particular constant input, $\boldsymbol{o}$, an RNN is at a *fixed point* when $\| f_\phi(\boldsymbol{z}, \boldsymbol{o}) - \boldsymbol{z} \|_2^2 \approx 0$. Numerically, we can simply look for $\boldsymbol{z}$ where $\| f_\phi(\boldsymbol{z}, \boldsymbol{o}) - \boldsymbol{z} \|_2^2 < \epsilon$. For our analyses below we chose $\epsilon = 1 \times 10^{-5}$.

Identifying fixed points (Figs 5B and 7G).   During training, RNNs received three distinct types of inputs, $\boldsymbol{o}_t \in \{[0, 0], [1, 0], [0, r]\}$, which we refer to as the null ($\varnothing$), odor, and reward inputs, respectively. Under the beliefs of the Starkweather and Babayan tasks, the odor and reward inputs always result in a change in the beliefs. As a result, any fixed points of the beliefs must be conditional on the null input, $\varnothing$. We therefore sought to identify an RNN's fixed points conditional on a null input. To do this, we took a numerical approach: We initialized the RNN to a random state, applied the null input until the RNN's activity converged, and then repeated this process across different random states to get a candidate set of fixed points. More precisely, we considered $N = 20$ randomly selected values of $\boldsymbol{z}$ in the testing data following an odor or reward observation as a set of starting seeds. For each starting seed, $\boldsymbol{z}_0$, we computed the RNN's representation, $\boldsymbol{z}_t$, over time, given no further odor or reward observations: $\boldsymbol{z}_t = f_\phi(\boldsymbol{z}_{t-1}, \varnothing)$. We repeated this process until $\eta_t = \| \boldsymbol{z}_t - \boldsymbol{z}_{t-1} \|_2^2 < \epsilon$. We then added $\boldsymbol{z}_t$ to our list of candidate fixed points, $\mathcal{F}$. For each pair of candidate fixed points within a distance 1×10^{-3} of each other, we considered these to be the same fixed point.

Odor and reward memory duration ([Fig 5C and 5D](#)). For each Value RNN with a single fixed point, we measured the network's odor (or reward) memory as follows. We initialized each RNN to its fixed point, z_0, and then provided an odor (or reward) observation at time $t = 1$. We then measured the RNN's representation, z_t, over time, given no further odor or reward observations: $z_t = f_\phi(z_{t-1}, \varnothing)$, for $t > 1$. For each t, we calculated the distance of the activity from its fixed point: $\eta_t = \| z_t - z_0 \|_2^2$ ([Fig 5C](#)). We repeated this until η_t converged to zero, defining the *odor memory* (or *reward memory*) as the t at which $\eta_t < 1 \times 10^{-3}$ ([Fig 5D](#)).

Supporting information

S1 Fig. RNN activity before and after training on Starkweather Task 2. A. Example observations, states, beliefs, and Value RNN activity from the same Task 2 trials shown in Figs [2](#) and [4A](#). States and beliefs are colored as in [Fig 2](#), with black indicating ITI microstates, and other colors indicating ISI microstates. **B-C.** RNN unit activity (individually normalized to span between 0 and 1), with units sorted by time of peak activation on held-out trials, on an RNN before (panel **B**) and after (panel **C**) training. Both before and after after training, RNN units exhibited tuning to elapsed time following observations, with variance that scaled with elapsed time.
(TIF)

S2 Fig. Value RNNs trained on the Babayan task recapitulate dopamine activity and belief RPEs in response to intermediate reward sizes. A-B. Average dopamine response on trial 1 (panel **A**) and trial 2 (panel **B**) during probe sessions including blocks with intermediate reward sizes. Circles and lines depict mean ± SE across $N = 11$ animals. Reproduced from Babayan et al. (2018) [10]. **C-D.** Same as panels **A- B**, but for the RPEs of the Belief model (black) and Value RNNs (purple). Value RNNs were trained on sessions including only blocks with rewards $r_t \in \{1, 10\}$, as in the main text. Value weights for the Belief model and Value RNNs were fit using a test session including 39 blocks each with $r_t = 1$ and $r_t = 10$, and 3 blocks each with $r_t \in \{2, 4, 6, 8\}$, similar to the proportions used in Babayan et al. (2018) [10]. RPEs were then measured on a different test session. Purple circles and lines depict mean ± SE across $N = 12$ models.
(TIF)

S3 Fig. Value RNNs trained on the Babayan task exhibit one fixed point. A. RNN activity during two example trials, one during Block 1 (left) and the other during Block 2 (right). Same as [Fig 7D](#). Here we also include RNN activity trajectories if each reward had been omitted. While activity for the Block 2 trial initially returns to the putative ITI_2 state, it eventually returns to the true fixed point at ITI_1 **B.** Distance of RNN activity from the single fixed point (e.g., ITI_1 in panel **A**) following an odor observation (i.e., an omission trial). While the maximum ITI duration is theoretically infinite, the maximum ITI duration in the training data was at $t = 65$. RNN activity on Block 2 trials therefore remained separate from the activity on Block 1 trials for the range of experienced ITI durations.
(TIF)

S4 Fig. Performance of Value RNNs and Untrained RNNs as a function of added noise magnitude. A. Error between the RPEs of the Value RNN (dark purple) and Untrained RNN (light purple) relative to the Belief model's RPEs ("RPE MSE"; see [Fig 3D](#)) during Starkweather Task 2, as a function of the magnitude of the Gaussian noise added to each unit prior to analysis (see [Materials and methods](#)). All RNNs had 50 hidden units. Each dot is the error for a single Value RNN model. Each circle is the median across the $N = 12$ Value RNNs (dark purple) or $N = 12$ Untrained RNNs (light purple) at a given noise level. **B.** Total variance explained

(R^2) of beliefs on held-out trials (see Fig 4B). Same conventions as panel **A**. **C.** Cross-validated log-likelihood of the state decoder using RNN activity to estimate the true state (see Fig 4C). Same conventions as panel **A**.
(TIF)

Author Contributions

Conceptualization: Jay A. Hennig, Sandra A. Romero Pinto, Takahiro Yamaguchi, Scott W. Linderman, Naoshige Uchida, Samuel J. Gershman.

Formal analysis: Jay A. Hennig.

Funding acquisition: Scott W. Linderman, Naoshige Uchida, Samuel J. Gershman.

Investigation: Jay A. Hennig.

Methodology: Jay A. Hennig, Samuel J. Gershman.

Supervision: Scott W. Linderman, Naoshige Uchida, Samuel J. Gershman.

Visualization: Jay A. Hennig.

Writing – original draft: Jay A. Hennig.

Writing – review & editing: Jay A. Hennig, Sandra A. Romero Pinto, Takahiro Yamaguchi, Scott W. Linderman, Naoshige Uchida, Samuel J. Gershman.

References

1. Schultz W, Dayan P, Montague PR. A neural substrate of prediction and reward. Science. 1997; 275:1593–1599. https://doi.org/10.1126/science.275.5306.1593 PMID: 9054347

2. Bayer HM, Glimcher PW. Midbrain dopamine neurons encode a quantitative reward prediction error signal. Neuron. 2005; 47(1):129–141. https://doi.org/10.1016/j.neuron.2005.05.020 PMID: 15996553

3. Cohen JY, Haesler S, Vong L, Lowell BB, Uchida N. Neuron-type-specific signals for reward and punishment in the ventral tegmental area. nature. 2012; 482(7383):85–88. https://doi.org/10.1038/nature10754 PMID: 22258508

4. Eshel N, Bukwich M, Rao V, Hemmelder V, Tian J, Uchida N. Arithmetic and local circuitry underlying dopamine prediction errors. Nature. 2015; 525(7568):243–246. https://doi.org/10.1038/nature14855 PMID: 26322583

5. Kaelbling LP, Littman ML, Cassandra AR. Planning and acting in partially observable stochastic domains. Artificial intelligence. 1998; 101(1-2):99–134. https://doi.org/10.1016/S0004-3702(98)00023-X

6. Daw ND, Courville AC, Touretzky DS. Representation and timing in theories of the dopamine system. Neural computation. 2006; 18(7):1637–1677. https://doi.org/10.1162/neco.2006.18.7.1637 PMID: 16764517

7. Starkweather CK, Babayan BM, Uchida N, Gershman SJ. Dopamine reward prediction errors reflect hidden-state inference across time. Nature neuroscience. 2017; 20(4):581–589. https://doi.org/10.1038/nn.4520 PMID: 28263301

8. Lak A, Nomoto K, Keramati M, Sakagami M, Kepecs A. Midbrain dopamine neurons signal belief in choice accuracy during a perceptual decision. Current Biology. 2017; 27:821–832. https://doi.org/10.1016/j.cub.2017.02.026 PMID: 28285994

9. Sarno S, de Lafuente V, Romo R, Parga N. Dopamine reward prediction error signal codes the temporal evaluation of a perceptual decision report. Proceedings of the National Academy of Sciences. 2017; 114:E10494–E10503. https://doi.org/10.1073/pnas.1712479114 PMID: 29133424

10. Babayan BM, Uchida N, Gershman S, et al. Belief state representation in the dopamine system. Nature communications. 2018; 9(1):1–10. https://doi.org/10.1038/s41467-018-04397-0 PMID: 29760401

11. Mikhael JG, Kim HR, Uchida N, Gershman SJ. The role of state uncertainty in the dynamics of dopamine. Current Biology. 2022; 32:1077–1087. https://doi.org/10.1016/j.cub.2022.01.025 PMID: 35114098

12. Wilson RC, Takahashi YK, Schoenbaum G, Niv Y. Orbitofrontal cortex as a cognitive map of task space. Neuron. 2014; 81(2):267–279. https://doi.org/10.1016/j.neuron.2013.11.005 PMID: 24462094

13. Starkweather CK, Gershman SJ, Uchida N. The medial prefrontal cortex shapes dopamine reward prediction errors under state uncertainty. Neuron. 2018; 98(3):616–629. https://doi.org/10.1016/j.neuron.2018.03.036 PMID: 29656872

14. Gershman SJ, Uchida N. Believing in dopamine. Nature Reviews Neuroscience. 2019; 20:703–714. https://doi.org/10.1038/s41583-019-0220-7 PMID: 31570826

15. Pouget A, Beck JM, Ma WJ, Latham PE. Probabilistic brains: knowns and unknowns. Nature Neuroscience. 2013; 16(9):1170–1178. https://doi.org/10.1038/nn.3495 PMID: 23955561

16. Daw ND, Niv Y, Dayan P. Uncertainty-based competition between prefrontal and dorsolateral striatal systems for behavioral control. Nature Neuroscience. 2005; 8:1704–1711. https://doi.org/10.1038/nn1560 PMID: 16286932

17. Rao RP. Decision making under uncertainty: a neural model based on partially observable markov decision processes. Frontiers in computational neuroscience. 2010; 4:146. https://doi.org/10.3389/fncom.2010.00146 PMID: 21152255

18. Poupart P, Boutilier C. Value-directed compression of POMDPs. Advances in Neural Information Processing Systems. 2002; 15.

19. Roy N, Gordon G, Thrun S. Finding approximate POMDP solutions through belief compression. Journal of Artificial Intelligence Research. 2005; 23:1–40. https://doi.org/10.1016/j.artint.2005.06.002

20. Botvinick M, Wang JX, Dabney W, Miller KJ, Kurth-Nelson Z. Deep reinforcement learning and its neuroscientific implications. Neuron. 2020; 107(4):603–616. https://doi.org/10.1016/j.neuron.2020.06.014 PMID: 32663439

21. Ni T, Eysenbach B, Salakhutdinov R. Recurrent Model-Free RL Can Be a Strong Baseline for Many POMDPs. In: Chaudhuri K, Jegelka S, Song L, Szepesvari C, Niu G, Sabato S, editors. Proceedings of the 39th International Conference on Machine Learning. vol. 162 of Proceedings of Machine Learning Research. PMLR; 2022. p. 16691–16723.

22. Gershman SJ, Daw ND. Reinforcement learning and episodic memory in humans and animals: an integrative framework. Annual Review of Psychology. 2017; 68:101–128. https://doi.org/10.1146/annurev-psych-122414-033625 PMID: 27618944

23. Cho K, Van Merriënboer B, Gulcehre C, Bahdanau D, Bougares F, Schwenk H, et al. Learning phrase representations using RNN encoder-decoder for statistical machine translation. arXiv preprint arXiv:14061078. 2014;.

24. Sussillo D, Barak O. Opening the black box: low-dimensional dynamics in high-dimensional recurrent neural networks. Neural computation. 2013; 25(3):626–649. https://doi.org/10.1162/NECO_a_00409 PMID: 23272922

25. Maheswaranathan N, Williams A, Golub M, Ganguli S, Sussillo D. Universality and individuality in neural dynamics across large populations of recurrent networks. Advances in neural information processing systems. 2019; 32. PMID: 32782422

26. Vyas S, Golub MD, Sussillo D, Shenoy KV. Computation through neural population dynamics. Annual review of neuroscience. 2020; 43:249–275. https://doi.org/10.1146/annurev-neuro-092619-094115 PMID: 32640928

27. Jaeger H. Echo state network. scholarpedia. 2007; 2(9):2330. https://doi.org/10.4249/scholarpedia.2330

28. Lukoševičius M, Jaeger H. Reservoir computing approaches to recurrent neural network training. Computer science review. 2009; 3(3):127–149. https://doi.org/10.1016/j.cosrev.2009.03.005

29. Saxe AM, McClelland JL, Ganguli S. Exact solutions to the nonlinear dynamics of learning in deep linear neural networks. arXiv preprint arXiv:13126120. 2013;.

30. Merel J, Aldarondo D, Marshall J, Tassa Y, Wayne G, Ölveczky B. Deep neuroethology of a virtual rodent. arXiv preprint arXiv:191109451. 2019;.

31. Xu T, Barak O. Implementing Inductive bias for different navigation tasks through diverse RNN attractors. arXiv preprint arXiv:200202496. 2020;.

32. Zhang R, Pitkow X, Angelaki DE. Inductive biases of neural networks for generalization in spatial navigation. bioRxiv. 2022; p. 2022–12.

33. Singh SH, van Breugel F, Rao RP, Brunton BW. Emergent behaviour and neural dynamics in artificial agents tracking odour plumes. Nature Machine Intelligence. 2023; 5(1):58–70. https://doi.org/10.1038/s42256-022-00599-w

34. Wu Z, Kwon M, Daptardar S, Schrater P, Pitkow X. Rational thoughts in neural codes. Proceedings of the National Academy of Sciences. 2020; 117(47):29311–29320. https://doi.org/10.1073/pnas.1912336117 PMID: 33229521

35. Wang JX, Kurth-Nelson Z, Kumaran D, Tirumala D, Soyer H, Leibo JZ, et al. Prefrontal cortex as a meta-reinforcement learning system. Nature neuroscience. 2018; 21(6):860–868. https://doi.org/10.1038/s41593-018-0147-8 PMID: 29760527

36. Mikulik V, Delétang G, McGrath T, Genewein T, Martic M, Legg S, et al. Meta-trained agents implement bayes-optimal agents. Advances in neural information processing systems. 2020; 33:18691–18703.

37. Lambrechts G, Bolland A, Ernst D. Recurrent networks, hidden states and beliefs in partially observable environments. Transactions on Machine Learning Research. 2022;.

38. Smith J, Linderman S, Sussillo D. Reverse engineering recurrent neural networks with Jacobian switching linear dynamical systems. Advances in Neural Information Processing Systems. 2021; 34:16700–16713.

39. Gershman SJ, Moustafa AA, Ludvig EA. Time representation in reinforcement learning models of the basal ganglia. Frontiers in computational neuroscience. 2014; 7:194. https://doi.org/10.3389/fncom.2013.00194 PMID: 24409138

40. Namboodiri VMK. How do real animals account for the passage of time during associative learning? Behavioral Neuroscience. 2022;. https://doi.org/10.1037/bne0000516 PMID: 35482634

41. Ludvig EA, Sutton RS, Kehoe EJ. Stimulus representation and the timing of reward-prediction errors in models of the dopamine system. Neural Computation. 2008; 20:3034–3054. https://doi.org/10.1162/neco.2008.11-07-654 PMID: 18624657

42. Mello GB, Soares S, Paton JJ. A scalable population code for time in the striatum. Current Biology. 2015; 25:1113–1122. https://doi.org/10.1016/j.cub.2015.02.036 PMID: 25913405

43. MacDonald CJ, Lepage KQ, Eden UT, Eichenbaum H. Hippocampal "time cells" bridge the gap in memory for discontiguous events. Neuron. 2011; 71:737–749. https://doi.org/10.1016/j.neuron.2011.07.012 PMID: 21867888

44. Tiganj Z, Jung MW, Kim J, Howard MW. Sequential firing codes for time in rodent medial prefrontal cortex. Cerebral Cortex. 2017; 27:5663–5671. https://doi.org/10.1093/cercor/bhw336 PMID: 29145670

45. Paton JJ, Buonomano DV. The neural basis of timing: distributed mechanisms for diverse functions. Neuron. 2018; 98(4):687–705. https://doi.org/10.1016/j.neuron.2018.03.045 PMID: 29772201

46. Littman M, Sutton RS. Predictive representations of state. Advances in neural information processing systems. 2001; 14.

47. Hochreiter S. The vanishing gradient problem during learning recurrent neural nets and problem solutions. International Journal of Uncertainty, Fuzziness and Knowledge-Based Systems. 1998; 6 (02):107–116. https://doi.org/10.1142/S0218488598000094

48. Glorot X, Bengio Y. Understanding the difficulty of training deep feedforward neural networks. In: Proceedings of the thirteenth international conference on artificial intelligence and statistics. JMLR Workshop and Conference Proceedings; 2010. p. 249–256.

49. Sutton RS, Barto AG. Reinforcement learning: An introduction. MIT press; 2018.